POR-2026(EX)
(WT-2026)(EX)
EXTRACTED VERSION

OPERATION DOMINIC, FISH BOWL SERIES

Project Officer's Report—Project 6.7

Debris Expansion Experiment

P. Dyal, Project Officer
W. Simmons
Air Force Weapons Laboratory
Kirtland AFB, NM

10 December 1965

NOTICE:
This is an extract of POR-2026 (WT-2026), Operation DOMINIC, Fish Bowl Series, Project 6.7.

Extracted version prepared for
Director
DEFENSE NUCLEAR AGENCY
Washington, DC 20305-1000

1 September 1985

UNCLASSIFIED
SECURITY CLASSIFICATION OF THIS PAGE

AD-A195428

REPORT DOCUMENTATION PAGE

1a. REPORT SECURITY CLASSIFICATION UNCLASSIFIED	1b. RESTRICTIVE MARKINGS
2a. SECURITY CLASSIFICATION AUTHORITY	3. DISTRIBUTION/AVAILABILITY OF REPORT Approved for public release; distribution is unlimited.
2b. DECLASSIFICATION/DOWNGRADING SCHEDULE	
4. PERFORMING ORGANIZATION REPORT NUMBER(S)	5. MONITORING ORGANIZATION REPORT NUMBER(S) POR-2026 (EX) (WT-2026) (EX)
6a. NAME OF PERFORMING ORGANIZATION Air Force Weapons Laboratory 6b. OFFICE SYMBOL (If applicable)	7a. NAME OF MONITORING ORGANIZATION Defense Atomic Support Agency
6c. ADDRESS (City, State, and ZIP Code) Kirtland AFB, NM	7b. ADDRESS (City, State, and ZIP Code) Washington, DC
8a. NAME OF FUNDING/SPONSORING ORGANIZATION 8b. OFFICE SYMBOL (If applicable)	9. PROCUREMENT INSTRUMENT IDENTIFICATION NUMBER
8c. ADDRESS (City, State, and ZIP Code)	10. SOURCE OF FUNDING NUMBERS PROGRAM ELEMENT NO. / PROJECT NO. / TASK NO. / WORK UNIT ACCESSION NO.

11. TITLE (Include Security Classification)
OPERATION DOMINIC, FISH BOWL SERIES, PROJECT OFFICER'S REPORT; PROJECT 6.7 - Debris Expansion Experiment, Extracted Version

12. PERSONAL AUTHOR(S)
P. Dyal and W. Simmons

13a. TYPE OF REPORT	13b. TIME COVERED FROM ____ TO ____	14. DATE OF REPORT (Year, Month, Day)	15. PAGE COUNT
		651210	96

16. SUPPLEMENTARY NOTATION This report has had sensitive military information removed in order to provide an unclassified version for unlimited distribution. The work was performed by the Defense Nuclear Agency in support of the DoD Nuclear Test Personnel Review Program.

17. COSATI CODES			18. SUBJECT TERMS (Continue on reverse if necessary and identify by block number)
FIELD	GROUP	SUB-GROUP	Dominic, Debris Expansion, Fish Bowl, Atomic Clouds
18	3		

19. ABSTRACT (Continue on reverse if necessary and identify by block number)

This experiment was designed to measure the interaction of expanding nuclear weapon debris with the ion-loaded geomagnetic field. Five rockets on Star Fish and two rockets on Check Mate were used to position instrumented payloads at various distances around the burst points. The instruments measured the magnetic field, ion flux, beta flux, gamma flux, and the neutron flux as a function of time and space around the detonations. Data was transmitted at both real and recorded times to island receiving sites near the burst regions. Measurements of the telemetry signal strengths at these sites allowed observations of blackout at 250 Mc.

Data reduction indicates that the early expansion of the Star Fish debris probably took the form of an ellipsoid with its major axis oriented along the earth's magnetic field lines. Collapse of the magnetic bubble was complete in approximately 16 seconds, and part of the fission fragment beta particles were subsequently injected into trapped orbits.

20. DISTRIBUTION/AVAILABILITY OF ABSTRACT	21. ABSTRACT SECURITY CLASSIFICATION
☒ UNCLASSIFIED/UNLIMITED ☐ SAME AS RPT. ☐ DTIC USERS	UNCLASSIFIED

22a. NAME OF RESPONSIBLE INDIVIDUAL	22b. TELEPHONE (Include Area Code)	22c. OFFICE SYMBOL
MARK D. FLOHR	202-325-7559	DNA/ISCM

DD FORM 1473, 84 MAR — 83 APR edition may be used until exhausted. All other editions are obsolete.

SECURITY CLASSIFICATION OF THIS PAGE
UNCLASSIFIED

FOREWORD

Classified material has been removed in order to make the information available on an unclassified, open publication basis, to any interested parties. The effort to declassify this report has been accomplished specifically to support the Department of Defense Nuclear Test Personnel Review (NTPR) Program. The objective is to facilitate studies of the low levels of radiation received by some individuals during the atmospheric nuclear test program by making as much information as possible available to all interested parties.

The material which has been deleted is either currently classified as Restricted Data or Formerly Restricted Data under the provisions of the Atomic Energy Act of 1954 (as amended), or is National Security Information, or has been determined to be critical military information which could reveal system or equipment vulnerabilities and is, therefore, not appropriate for open publication.

The Defense Nuclear Agency (DNA) believes that though all classified material has been deleted, the report accurately portrays the contents of the original. DNA also believes that the deleted material is of little or no significance to studies into the amounts, or types, of radiation received by any individuals during the atmospheric nuclear test program.

OPERATION DOMINIC

FISH-BOWL SERIES

PROJECT OFFICERS REPORT—PROJECT 6.7

DEBRIS EXPANSION EXPERIMENT

P. Dyal, Project Officer
W. Simmons, Captain, USAF

Air Force Weapons Laboratory
Kirtland AFB, New Mexico

ABSTRACT

This experiment was designed to measure the interaction of expanding nuclear weapon debris with the ion-loaded geomagnetic field.

Five rockets on Star Fish and two rockets on Check Mate were used to position instrumented payloads at various distances around the burst points. The instruments measured the magnetic field, ion flux, beta flux, gamma flux, and the neutron flux as a function of time and space around the detonations. Data was transmitted at both real and recorded times to island receiving sites near the burst regions. Measurements of the telemetry signal strengths at these sites allowed observations of blackout at 250 Mc.

Data reduction, which is currently being conducted at the Air Force Weapons Laboratory, indicates that the early expansion of the Star Fish debris probably took the form of an ellipsoid with its major axis oriented along the earth's magnetic field lines. Collapse of the magnetic bubble was complete in approximately 16 seconds, and part of the fission fragment beta particles were subsequently injected into trapped orbits.

PREFACE

The authors wish to express their appreciation for the guidance and contributions of the following people during the planning, buildup, and execution phase of this experiment:

Col Lew Allen

Mr. Robert G. Bland

Mr. Edward L. Breen

Col Kenneth R. Chapman

Lt J. D. Garcia

Mr. Martin Havens

Mr. Charles Hale

Capt David P. Milnor

AlC James V. Murray

Lt Billy R. Parker

Lt Robert Reynolds

Lt Dave Thompson

Capt William A. Whitaker

Mr. Thomas Yium

CONTENTS

TABLES

FIGURES

CHAPTER 1

INTRODUCTION

1.1 OBJECTIVES

The primary objective of this project was to measure the characteristics of the expanding Star Fish debris which were pertinent to weapon effects. The Star Fish nuclear explosion occurred at an altitude of 400 kilometers with a yield of approximately 1.15 megatons, and the event was considered to be above the atmosphere insofar as familiar sea level phenomena are concerned. The most important energy loss mechanism for the exploding material at this altitude is its interaction with the ion-loaded geomagnetic field. This experiment measured the magnetic field, ion density, gamma flux, neutron flux, and fission fragment beta flux in order to obtain a better understanding of the weapon debris expansion. A secondary objective was to observe the formation of the Argus shell of fission beta particles. Attenuation measurements of the 250-megacycle telemetry signals propagated through the ionized regions also permitted a direct observation of blackout effects due to gammas, neutrons, and the debris pancake (Reference 1).

1.2 BACKGROUND AND THEORY

Sea level nuclear burst phenomena can be adequately described by classical hydrodynamics. The low-energy X-rays and detonation products, which represent over 90% of the bomb's energy, interact with the surrounding air, and the resulting shock phenomena are

described in Reference 2. The conditions behind the normal shock wave are determined by laws of conservation of mass, momentum, and energy

$$P = P_1 + \rho_1 U_s^2 (1 - \rho_1/\rho)$$

$$H = H_1 + 1/2\ U_s^2 \left(1 - (\rho_1/\rho)^2 \right)$$

where P, ρ, and H are pressure, density and enthalpy of the gas, respectively. The shock velocity is denoted by U_s, and the suffix 1 denotes conditions in the undisturbed gas ahead of the shock wave. It is apparent that the most important mechanism of containment is the surrounding mass of cool air.

At altitudes above 200 kilometers, the burst phenomena of nuclear weapons is completely different. There is little air in this region for coupling of the energy of the detonation products, and as a result, the particles travel unimpeded for several thousands of kilometers. During the early phase of a high-altitude explosion, a large percentage of the detonation products is ionized and can therefore interact with the geomagnetic field and can also undergo Coulomb scattering with the ambient air atoms. If the expansion is high enough above the atmosphere, an Argus shell of electrons can be formed as in the 1958 and 1962 test series. The theory describing the motion of a plasma in a magnetic field is described in References 3 and 4. The equation of motion of a plasma expanding in a magnetic field is

$$\rho \delta v/\delta t = - \nabla (P + B^2/8\pi) + B \cdot \nabla B/4\pi$$

where v, t, and B are the velocity, time, and magnetic field, respectively. The quantities which are least known in such a plasma expansion are the state of ionization and the radial velocity distribution of the debris. If this velocity of the plasma is greater than the local sound or Alfven speed, a magnetic shock similar to a hydro shock can be formed which dissipates a sizable fraction of the plasma kinetic energy. The Alfven velocity is

$$C_A = B(4\pi\rho)^{-1/2}$$

where C_A is the Alfven velocity in cm/sec

B is the magnetic field in gauss

ρ is the ion density in ions/cm^3

Since the Star Fish debris expansion was predicted and measured to be approximately 2×10^8 cm/sec and the Alfven velocity is about 2×10^7 cm/sec, a shock should be formed. A consideration of the conservation of momentum and energy indicates that the total extent of the plasma expansion proceeds until the weapon plasma kinetic energy is balanced by the $B^2/8\pi$ magnetic field energy in the excluded region and the energy of the air molecules picked up by the expanding debris.

1.3 STAR FISH

The Star Fish device was detonated at an altitude of 400.09 kilometers and had a total weight of The yield was and the detonation time was 32409.029 seconds Zulu on 9 July 1962 (Reference 5). Preshot calculating in Reference 6 predicted that kinetic energy would be in the bomb debris at 2 microseconds.

A sequential history of the plasma expansion proceeds as follows:

The radioactive debris which rises to extreme altitudes will form a trapped belt of electrons around the earth. The debris which is deposited on top of the atmosphere will decay and ionize the air, causing attenuation of RF signals, aurora, etc.

An estimate of the maximum radial extent of the Star Fish magnetic bubble can be made assuming conservation of momentum and energy. The magnetic field swept along by the plasma electrons will pick up ambient air ions as it proceeds outward. Denote the mass per steradian of air ions by $M_{air}/4\pi$ and the mass of the bomb per steradian by $M_B/4\pi$. Conservation of momentum gives

$$\left(\frac{M_B}{4\pi} + \frac{M_{air}}{4\pi}\right) V = \frac{M_B}{4\pi} V_B$$

where V_B is the initial expansion velocity of the debris. The initial kinetic energy is given by

$$KE = \frac{1}{2} M_B V_B^2$$

The debris energy density can be equated to the energy density in the magnetic field and is given by

$$\frac{4}{3}\pi R^3 \frac{B^2}{8\pi} = \frac{1}{2} (M_{air} + M_B) V^2$$

Eliminating V from both equations

$$R^3 = \frac{3 V_B^2 M_B^2}{B^2 (M_{air} + M_B)}$$

Both the air mass M_{air} and the geomagnetic field B are functions of R, the radius of expansion. Using the ion density given in Reference 7 and magnetic field variations as $B = \frac{Bo}{R^3} (1 + 3 \cos^2\theta)^{1/2}$,

a table of maximum radial extension of the ionized debris was calculated to be as follows:

DIRECTION OF MOTION	PERCENTAGE DEBRIS IONIZED 100% km	10% km	1% km
Horizontal (400 km)	550	260	120
Upward Perpendicular to Field	980	350	140
Downward Perpendicular to Field	285	210	100

These values assume that the expansion is spherically symmetric, that the ion densities are as predicted in Reference 7 and that the state of ionization is frozen-in after a few microseconds of expansion time. It is also assumed that only ions are picked up by the expanding debris and field. These approximate distances were used as guides in the positioning of instruments to measure the percentage of the debris which would remain effectively ionized.

1.4 CHECK MATE

Expansion of the debris was mostly determined by the surrounding atmosphere which had a density of 4.8×10^{10} particles/cm^3.

CHAPTER 2

PROCEDURE

2.1 OPERATIONS

2.1.1 Star Fish. The Star Fish weapon was positioned in space using a Thor rocket. Timing coordination to 1-second accuracy was important since experimental payloads were positioned around the weapon at detonation time. The Thor engines were ignited, and the retaining locks held the missile on the pad until proper engine thrust was obtained. The uncertainty in Thor take-off time due to this unknown thrust was approximately 12 seconds, and H-0 time was readjusted at Thor lift-off. The Thor left the pad at H-821 seconds, then separated from the nose cone containing the bomb. The bomb was detonated at an altitude of 400 kilometers. Project 6.7 had five rockets which took off at H-510, 462, 266, 160, and 140 seconds, respectively, and positioned the instrumented payloads around the weapon at H-0 time. With these take-off times the experimental payloads and rockets could have been saved if the weapon had been aborted before H−515 seconds.

The rocket trajectories are shown in Figure 2.1. This figure represents a slice in the magnetic meridian through Johnston Island using the expression in Reference 10 for the geomagnetic field. The rocket positions at H−0 time are denoted by extra heavy lines. The length of these lines repre-

sents the 30 seconds of data which was recorded after H−0. The sequence of events for each one of these rockets was as follows:

(1) The three first-stage motors were ignited, and the rocket left the pad.

(2) The first stage burned out in 36 seconds, and the rocket coasted out of the atmosphere for about 15 seconds.

(3) The second stage was ignited, separated from the first stage, and boosted the payload up to the proper velocity.

(4) After second-stage burnout, the nose cone was ejected forward and away from the payload.

(5) The rubidium magnetometer was then telescoped approximately 5 feet away from the rest of the payload.

(6) The payload proceeded to its predetermined position at H-0.

(7) The weapon detonated, and the prompt gammas from the device triggered the tape recorder timer.

(8) Thirty seconds of high-frequency data was recorded.

(9) The timer turned off the erase mode, and the thirty seconds of data was continuously played back through a telemetry transmitter to receiver stations on the earth's surface. Three real-time channel measurements were transmitted to the receiving sites during the entire flight simultaneously with the recorded information.

Radiation and material arrived at the instrumented rocket positions in a time sequence which depended on the properties of the device and the surrounding medium. Project 6.7 paylcads located

in the hard vacuum surrounding the Star Fish device detected the weapon phenomena in the following sequence:

(1) Prompt gammas from the neutron interactions with bomb material and from the fission events.

(2) X-rays from the case material.

(3) 14-Mev neutrons from the fusion events during weapon burning.

(4) Low-energy neutrons from fission events, high-energy beta particles from fission fragments and case material.

(5) Radioactive bomb debris.

(6) Ionized air.

(7) Argus trapped beta particles.

The arrival times of the above radiations are strongly dependent on the position of the instruments with respect to the bomb, the magnetic field, and the ambient material between the bomb and instruments. At later times, the radioactive debris deposits on top of the atmosphere and causes blackout of payload telemetry signals passing through this ionized region (Reference 1).

2.1.2 Check Mate. The Check Mate device was positioned in space with the Strypi vehicle which uses the same rocket motor as the first stage of Project 6.7 SWIK vehicles. Due to the common flight properties of these rockets, there was no chance to save the experimental payloads and rockets in case of a weapon abort. Two payloads were positioned around the Check Mate device, and their positions at H-0 are shown in Figure 3.16. The rocket and measurement sequence for Check Mate was the same as described previously

for Star Fish. The weapon phenomenology was quite different, however, since the surrounding air was dominant in containing the expansion as contrasted to the magnetic field containment of Star Fish.

2.2 INSTRUMENTATION

2.2.1 Rockets and Instrument Placement. The rocket used to position the scientific instruments was a spin-stabilized, two-stage, solid-propellant vehicle. The rocket was 36 feet long, weighed 13,000 pounds, and boosted a 430-pound payload to an altitude of 1,200 kilometers. The first stage consisted of three motors (two X-19 Recruits and one XM-33) which were fabricated by the Thiokol Company. The two Thiokol Recruits were used to initially assist boost off the zero-length rail launcher, and each generated 35,000 pounds of thrust for 1.5 seconds. The Recruit motor had a gross weight of 348 pounds and was 102 inches long and 9 inches in diameter. The Thiokol XM-33 generated 50,000 pounds of thrust for 33 seconds. It weighed 8,732 pounds and was 232 inches long and 31 inches in diameter. An Allegheny Company X-254 motor was used for the second stage of the SWIK rocket. It weighed 2,085 pounds and was 116 inches long and 31 inches in diameter. It generated 12,000 pounds of thrust for 38 seconds. The exterior hardware including the fins, nose cone, etc., was designed and constructed by Atlantic Research Corporation. The rocket was launched from a zero-length rail; and by canting the fins, a spin rate of 2.5 cycles per second was obtained which remained constant during the vacuum coast part of the trajectory. The ablative nose cone was attached to the end of the second stage by a marmon clamp

which held 48 helical compressed springs. After the boost phase was over and the vehicle was out of the atmosphere, a timer released the marmon clamp, allowing the springs to eject the nose cone forward at a velocity of 16 feet per second. Immediately following nose cone ejection, a gas generator was fired which extended the telescope housing the rubidium magnetometer. Figure 2.5 shows the payload and spent second-stage motor as it existed during most of the flight time. A 2-Sigma dispersion of 32 mils was measured as the overall error in placement of scientific instruments. Trajectories for the five rockets in Star Fish are shown in Figure 2.1 and for the two rockets in Check Mate in Figure 3.16. These figures show the trajectories superimposed on a plane in the magnetic meridian through Johnston Island. The positions of the rockets at H-0 time are denoted by the short, heavy black line on each trajectory. Magnetic field lines in this meridian plane were determined from the equation for the geomagnetic field (Reference 10).
The rocket trajectories were programmed to follow the magnetic meridian as closely as possible. Figures 2.2 and 3.17 show the projection of the rocket trajectories upon the earth's surface for Star Fish and Check Mate, respectively. Figures 2.3 and 3.18 give the altitude of each rocket vs. time, and Figure 2.4 shows the rocket on the launcher before take-off.

2.2.2 Telemetry Receiving and Tracking. Due to the RF blackout problems at 250 megacycles, data was recorded in the payload and retransmitted to various receiving sites in the Pacific at Oahu, Hawaii, Tern, Johnston, and Canton Islands. Figure 2.2

shows the relative positions of these receiving sites with respect to the Star Fish trajectories. Kaena Point, Oahu, was run by the Pacific Missile Range and had two auto tracking antennas, and a TLM-18, 60-foot parabolic dish. The 60-foot dish had a 5-degree beam width with 28-db gain at 250 megacycles. Kaena Point received P-7 and P-2 on Star Fish and P-5 on the Check Mate event. South Point, Hawaii, was run by the Pacific Missile Range and also had a 60-foot TLM-18 dish which received P-6 during the Star Fish event. Tern Island had an auto tracking quad-helix run by the Pacific Missile Range and a manual track quad-helix operated by Air Force Weapons Laboratory (AFWL) personnel. Both quad-helix antennas had a gain of 19 db at 250 megacycles and a beam width of 18 degrees. The Tern Island facility received P-2 and P-7 for the Star Fish event and P-5 for the Check Mate event. Canton Island had two manual tracking quad-helix antennas; one operated as part of the Mercury Receiving Net out of AMR and one by AFWL personnel. These antennas had 19-db gain at 250 megacycles and an 18-degree beam width. Johnston Island had one small mono-helix antenna used for payload checkout. Since RF blackout was less than expected on Star Fish, the low-gain mono-helix antenna was able to receive some information on all five payloads. Due to this unexpected receiving ability, two quad-helix antennas were installed on Johnston Island for the Check Mate event. The receiving sites which possessed auto tracking capability gave enough data for trajectory determination based on time of flight and look angle information.

Cubic Corporation was contracted by DASA to transponder track

all small rockets from Johnston Island. One rocket was successfully tracked on Check Mate with Cubic's PME, AME equipment. RCA had a project on USAS American Mariner which was to have tracked a 5,776-megacycle transponder aboard P-6 Star Fish. This track was unsuccessful.

2.2.3 Instrumented Payload. The scientific payload weighed 433 pounds and was constructed almost entirely of non-magnetic materials. The cross-sectional view of the payload is shown in Figure 2.6 along with the position of the various instruments. A nylon cylinder which was 1.5 inches thick, 15 inches long, and 26 inches in diameter was used to enclose the electronics and shield the sensitive circuits from bremsstrahlung caused by high-energy beta particles. Since nylon is composed of relatively low Z materials, it is effective in minimizing the production of bremsstrahlung. The magnetometer was located at the end of a fiberglass telescope which was placed on top of the nylon cylinder so that magnetic gradients would be minimized in the gas cells of the magnetometer. The 10 watts of RF power radiated from the telemetry antennas, located directly below the nylon cylinder, was shielded out of the payload by a laminated copper-clad fiberglass shield. The block diagram for the electronics used in this experiment is shown in Figure 2.7. The left side of this figure shows the inputs from all the scientific instruments, and the right side shows the outputs to the antenna. The telemetry system was capable of transmitting 100-kc information, but the experiment required 200 kc bandwidth of information. This was obtained by recording two sets of data in a

tape recorder and time-sharing the output of this tape recorder into the telemetry system. Referring again to Figure 2.7, channels 4 through 18 were mixed and placed in channel 1 of the tape recorder, and the rubidium vapor magnetometer was simultaneously recorded in channel 2. A 40-second commutator was used to sequentially take the output of channel 1 and channel 2, mix this with channels 1 through 3 and transmit the information by frequency modulating a 250-megacycle carrier. The prompt gamma detector shown at the lower left hand corner of Figure 2.7 was used to control the record-erase functions of the tape recorder. A transponder operating at approximately 340 megacycles was supplied by Cubic Corporation for tracking purposes.

Power was supplied to the payload by three sets of batteries. The largest set consisted of 20 silver cells enclosed in a pressure-sealed fiberglass case which supplied 10 ampere-hours at 28 volts. The two other batteries consisted of a 300-volt and a 32-volt dry cell for biasing the Faraday cup grid and the solid-state detectors. Current drain on these batteries was less than 10 microamperes.

Telemetry for the entire payload was provided by an 18-channel FM/FM system which converted 0- to 5-volt instrument signal into 10 watts of RF power at 250 megacycles. The system had solid-state subcarrier oscillators and a ceramic tube power amplifier sealed in a vacuum-tight container. System distortion was less than 1 percent of the bandwidth in each channel. Built-in externally controlled calibration relays provided calibration of the entire system, and a 100-kc crystal-controlled oscillator was used as one subcarrier oscillator to remove wow and flutter produced by the tape recorder.

The transmitter fed a four-element, bent-stub antenna system which was set in teflon ablative material and mounted around the periphery of the payload. This antenna system was phased for right circular polarization when viewed from behind in the direction of flight. Frequencies for the seven payloads were 247.3, 237.0, 229.9, 221.5, and 229.9 megacycles for P-2, 3, 4, 6, and 7, respectively. Figure 2.5 shows the antenna positions on the payload during vehicle flight.

Due to complete loss of RF signal at H-0 time, a tape recorder was used to store information from H-5 seconds to H+25 seconds. This information was repeatedly played back through the transmitter to the receiving sites until splash. The recorder had two channels; each had a flat frequency response from 0.4 to 100 kilocycles and had wow and flutter less than 1 percent of the input signal. A timer which was started by a pulse from the prompt gamma detector was used to stop the record-erase function of the tape recorder after a preset time. This method allowed information recorded during blackout to be received at ground stations after the blackout had subsided or after the payload had cleared the blackout area.

The prompt gamma detector used three silicon solid-state detectors connected so that a coincidence from any two would trigger the tape recorder timer. These detectors were located near the center of the payload and had an area of one square centimeter, a resistivity of 4,000 ohms/cm and were biased at 60 volts. The circuit triggered on any gamma spike with a rise time less than 2×10^{-6} second, a flux rate greater than 2×10^{4} R/sec, and gamma ray energy approximately 1 Mev.

The gamma-neutron detector was a silicon solid-state detector of 1-cm^2 sensitive area and had a 5-decade log amplifier which converted 10^{-1} to 10^4 R/sec into 0 to 5 volts for the telemetry. It was located on the inside of the 1.5-inch-thick nylon cylinder, which shielded it from high-energy betas. Gamma rays are detected by photo-electric, Compton, and pair production interactions inside the depleted region of the silicon P-N junction. Gamma calibration was accomplished using a linear accelerator, the SPRF reactor, and a 4-kilocurie Co^{60} source. Neutrons are detected by measuring the recoil protons from the converter foil placed in front of the detector and by n^o,p and n^o,α reactions in the Si of the detector itself. Neutron energy calibrations have been completed, but the data reduction is still in progress. The time response of the detector and electronics is 10^{-5} second; therefore, the limiting time factor is the telemetry set which yields information from this detector to 10^{-3} second. Figure 2.11 shows the gamma-neutron detector without the polyethylene neutron-proton recoil foil.

Three Faraday cups were located 120 degrees apart on the periphery of the nylon cylinder, looking out at right angles to the payload spin axis. Each cup consisted of an outer grounded screen, a grid biased at -300 volts to reject thermal and secondary electrons, and an inner -300-volt grid biased to suppress secondary electrons from the foil and 0.56-inch-thick aluminum collector. The 0.001-inch-thick foil was designed to stop and measure the charged heavy debris ions, but electrons above 65 kev were transmitted to the thick 0.56-inch collector. The Faraday cups were calibrated with 0- to 10-Mev

electrons and 0- to 100-kev protons. The time response of the Faraday cup system was determined to be 10^{-4} second. Figure 2.10 shows the geometrical positions of the grids and foils.

Six beta detectors were located in the surface of the nylon payload (Figure 2.8). Three were located 120 degrees apart looking perpendicular to the payload spin axis, and three were located 120 degrees apart looking parallel to the spin axis. Each detector consisted of a 1-mm-thick, 0.25-cm^2 lithium ion drifted solid-state detector behind a 0.002-cm-thick aluminum foil. Figure 2.6 shows the position of the beta detectors looking parallel and perpendicular to the rocket spin axis. Each detector had a 60-degree look angle due to its recession into the nylon cylinder. The energy response to high-energy electrons is shown in Figure 2.9; the beta detector integrated this energy response, and the current output was fed into a 5-decade logarithmic amplifier. This detector amplifier system had a time response of 10^{-5} second. The telemetry system further limited this time response to 10^{-4} second. A time-varying fission beta energy spectra (Reference 11)

was used with the energy calibration to obtain the number of fission betas per cm^2 per second per steradian from the current output of the detector.

The Hall effect magnetometer was a solid-state multiplying device. The output voltage was proportional to the current flowing through the unit times the magnetic field perpendicular to the unit. The constant of proportionality is determined by the concentration of charge carriers and the sign of the carrier and their mobility.

The indium arsenide element used in this magnetometer had an output sensitivity of 10^{-1} volt per ampere control current per kilogauss field. A laminated mumetal flux concentrator enhanced this sensitivity by 10^{2}, and with an amplifier gain of 10^{3}, the magnetometer was capable of measuring magnetic fields from 0.03 to 4 gauss (plus and minus). The frequency response was limited by the telemetry to 10^{-4} second, and the instrument was positioned to measure the field vector along the vehicle spin axis. Figure 2.13 shows the Hall element and flux concentrator, and Figure 2.6 shows its position inside the payload.

The Rb^{85} magnetometer system utilized transitions between Zeeman sublevels in the ground state of the Rb^{85} atom in order to measure magnetic fields. The energy separation for the Zeeman splitting is proportional to the intensity of the magnetic field, and for Rb^{85} this is 4.67 cycles per second per 10^{-5} gauss magnetic field. An optical pumping technique was used to observe the quantum transitions which, in turn, yielded the intensity of the magnetic field. The output of the instrument was a 5-volt peak-to-peak sine wave varying in frequency from 0 to 467 kilocycles for magnetic fields from 0 to 1 gauss. Since the telemetry system could only transmit signals up to 100 kilocycles, a crystal-controlled oscillator was used to multiply the rubidium signal, and the low difference frequency was transmitted. Figure 2.12 shows the optical components of the magnetometer and Figure 2.6 shows the position of the magnetometer in the payload. Since a magnetic gradient of 10^{-4} gauss per centimeter along the optical axis of the instrument quenched the optical pumping process,

a nylon and fiberglass construction was used throughout the payload along with a telescoping device which moved the magnetometer away from current loops in the payload electronics. W. Whitaker calculated the largest eddy current loop allowable (at a position 70 inches from the electronic boxes) in order that the gradient in the magnetic field stay below 10^{-5} gauss per centimeter for large dB/dt. The frequency response of this system allowed field changes of 10^{4} gauss per second to be measured.

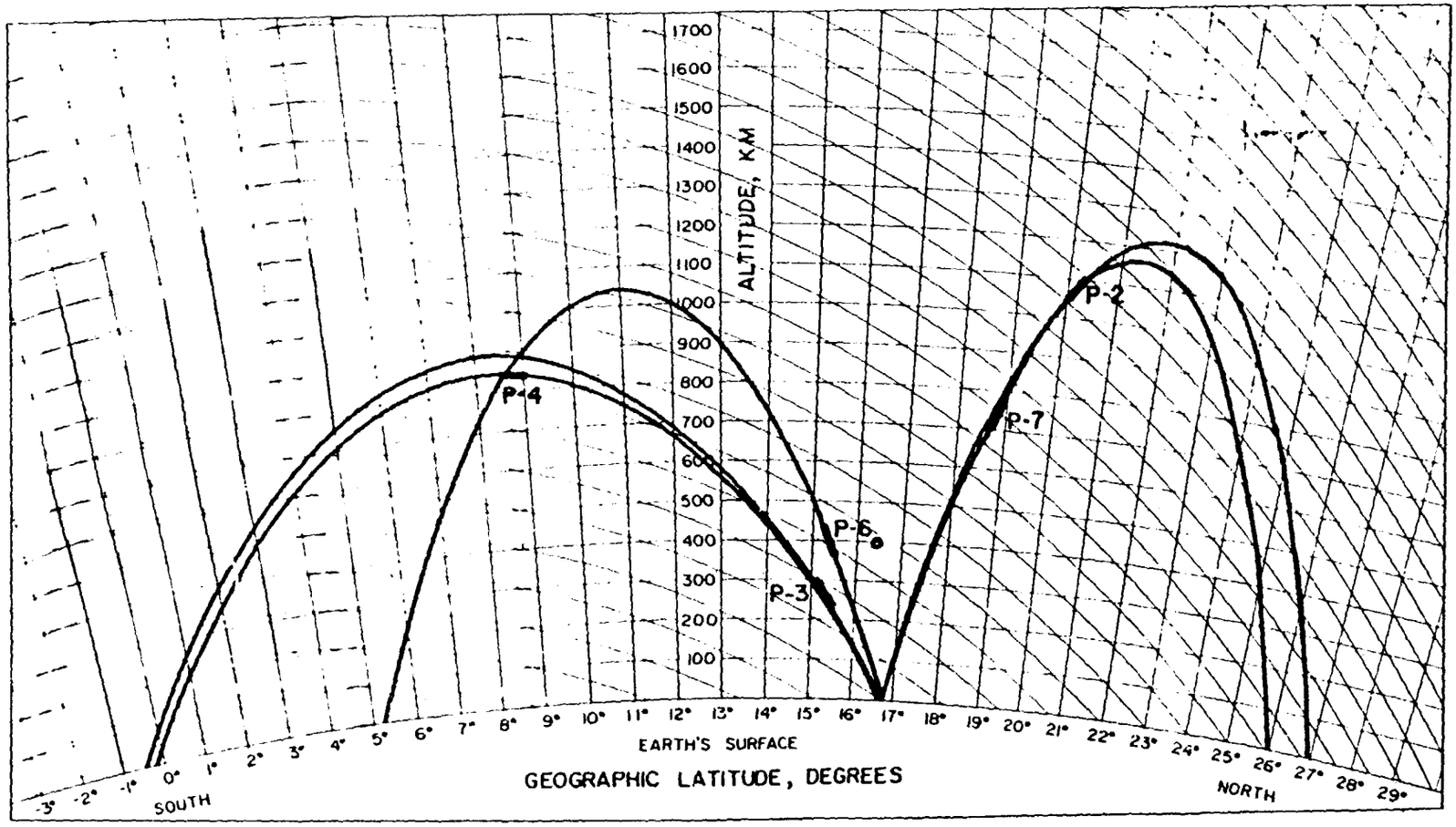

Figure 2.1 Star Fish rocket trajectories in magnetic meridian through Johnston Island.

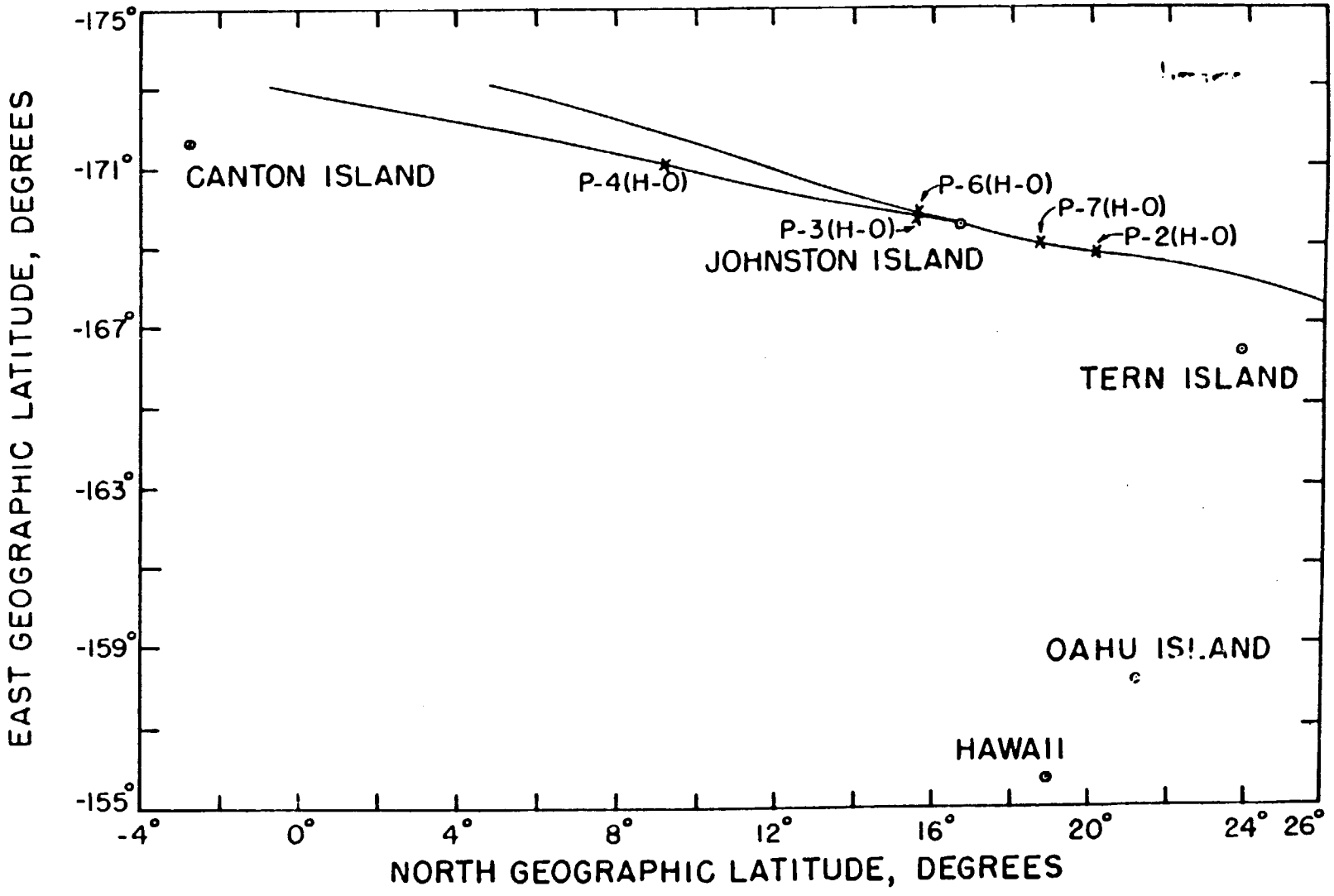

Figure 2.2 Star Fish rocket trajectories on earth's geographic surface.

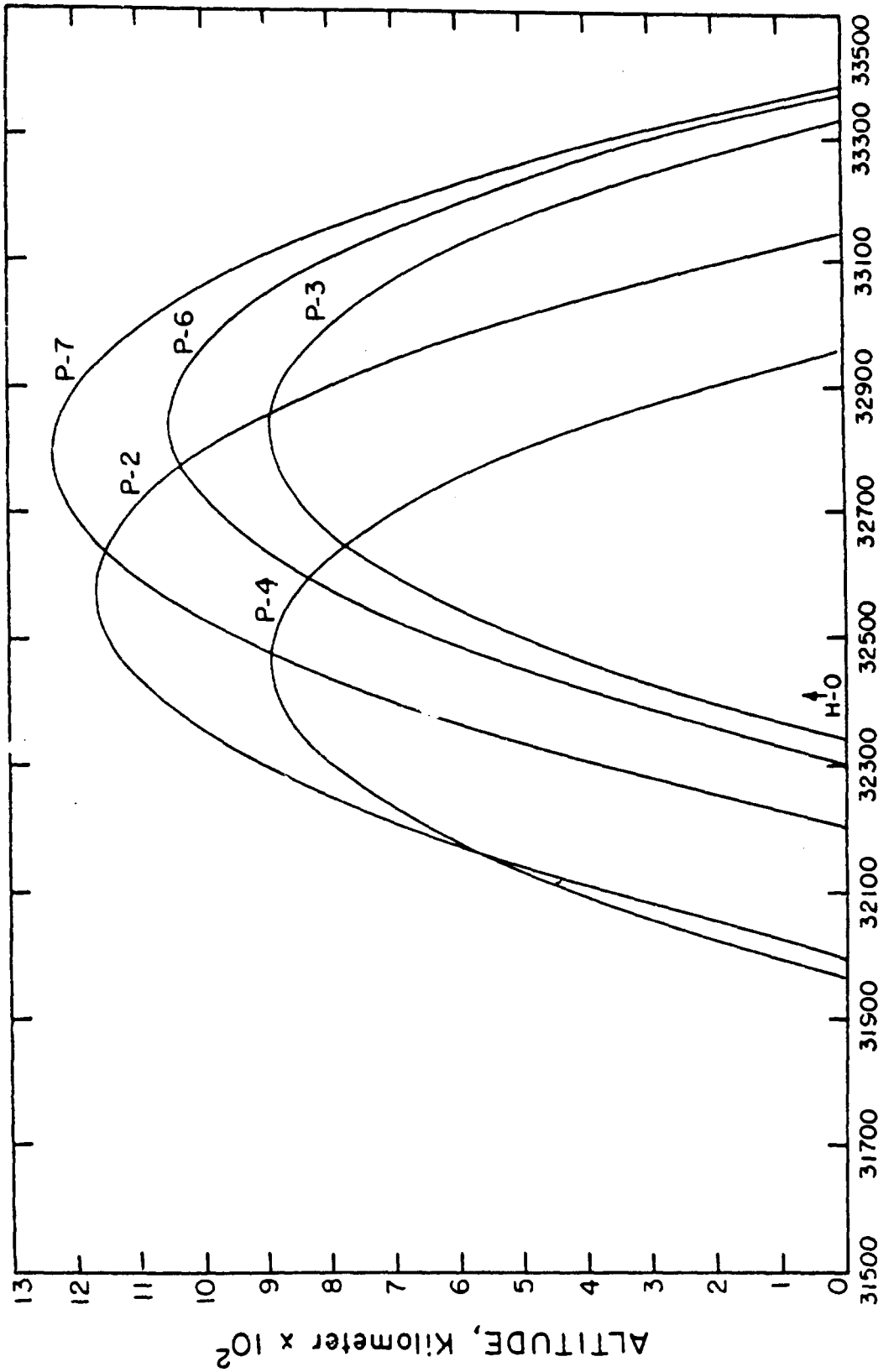

Figure 2.3 Star Fish altitude versus time.

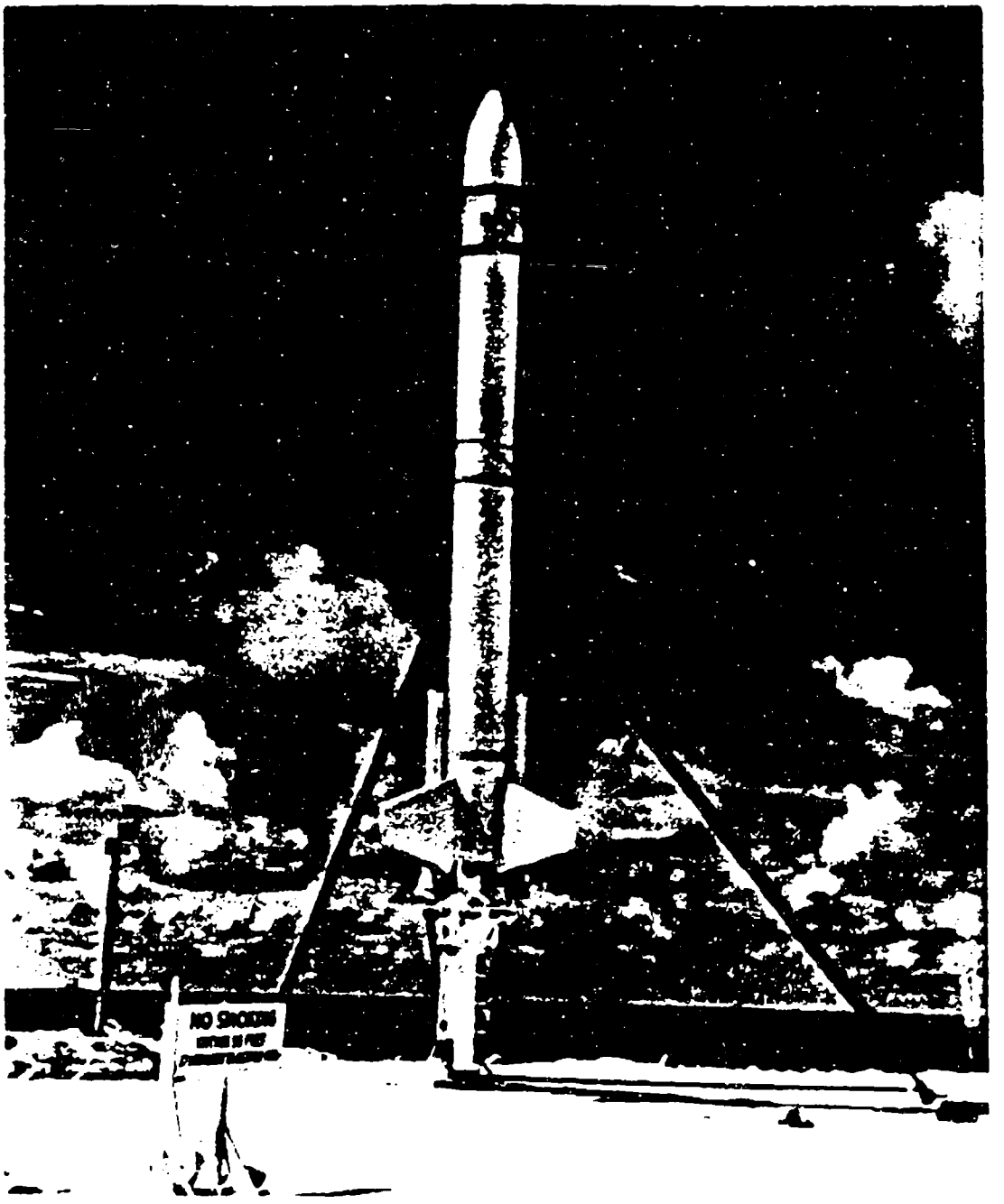

Figure 2.4 Rocket on launcher. (AFWL photo)

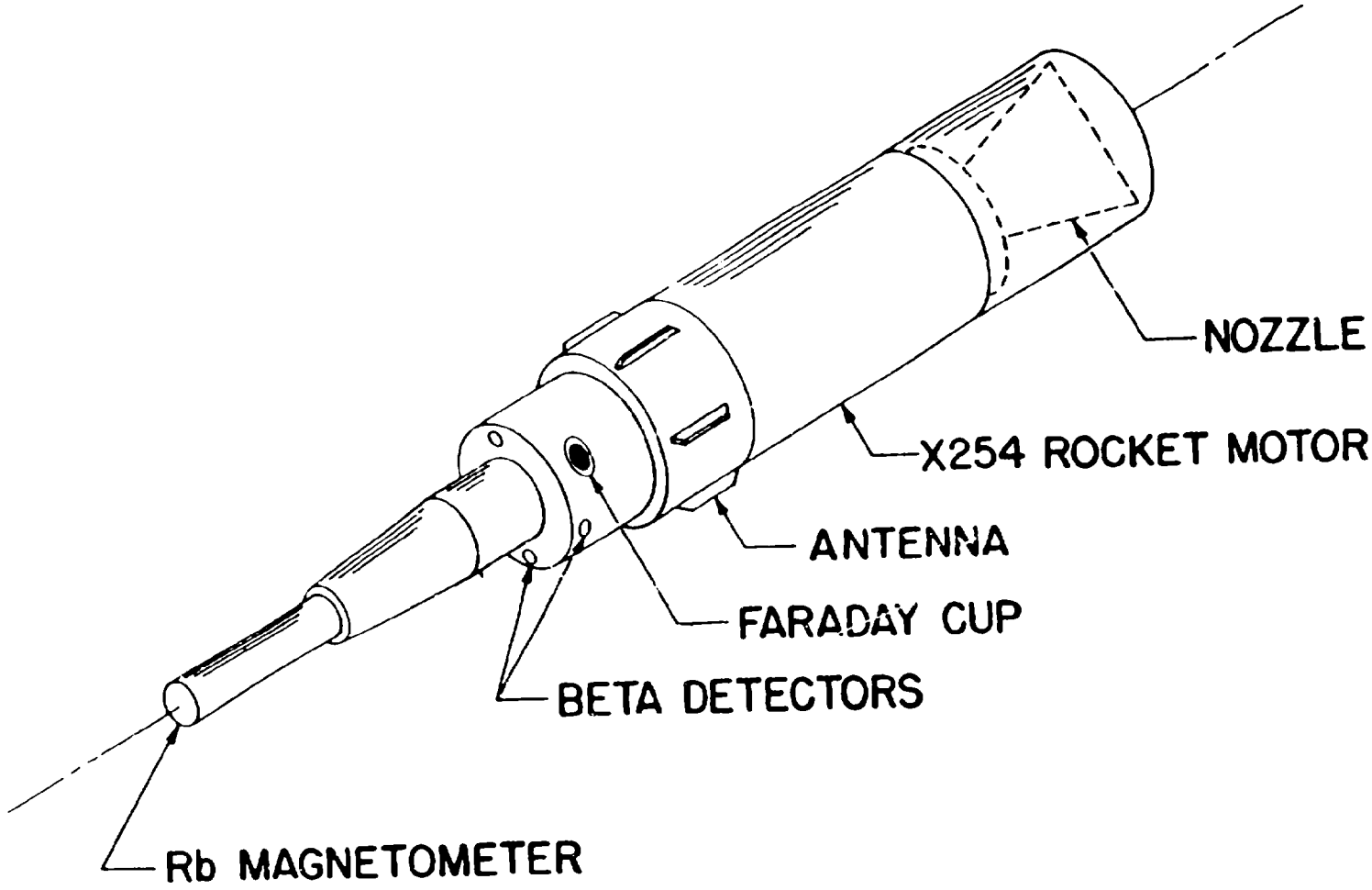

Figure 2.5 Rocket and payload in flight.

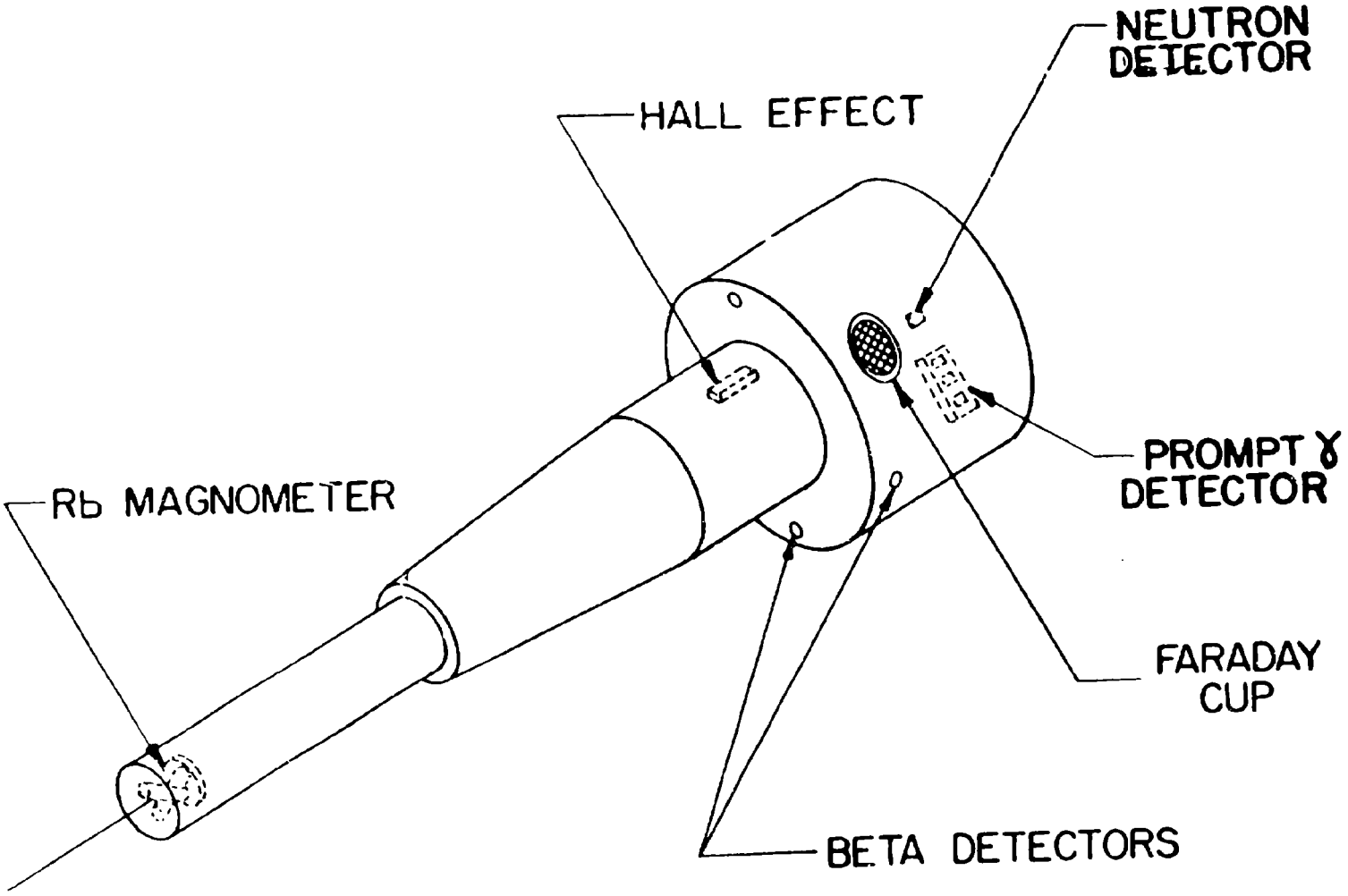

Figure 2.6 Cross section of payload.

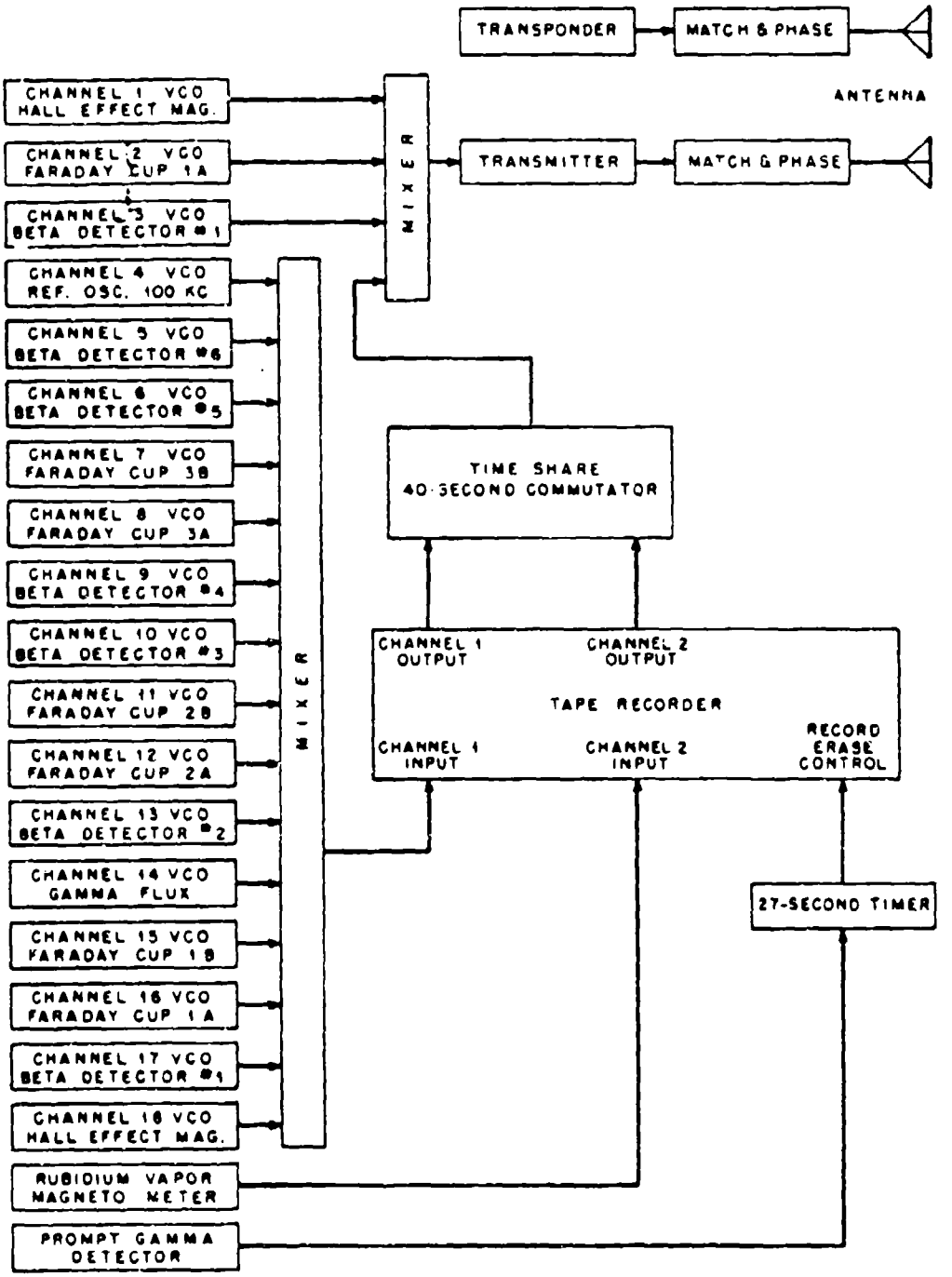

Figure 2.7 Block diagram.

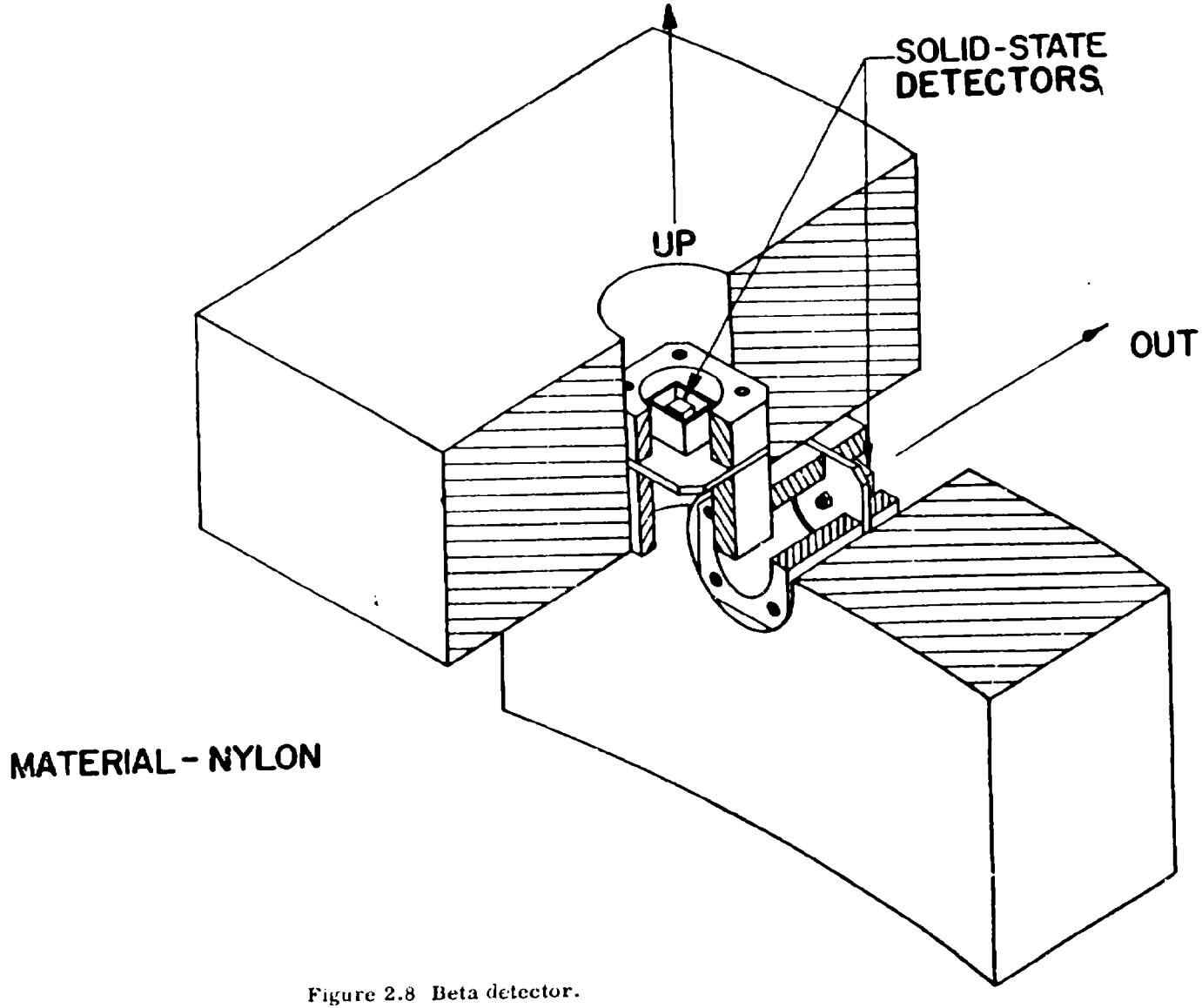

Figure 2.8 Beta detector.

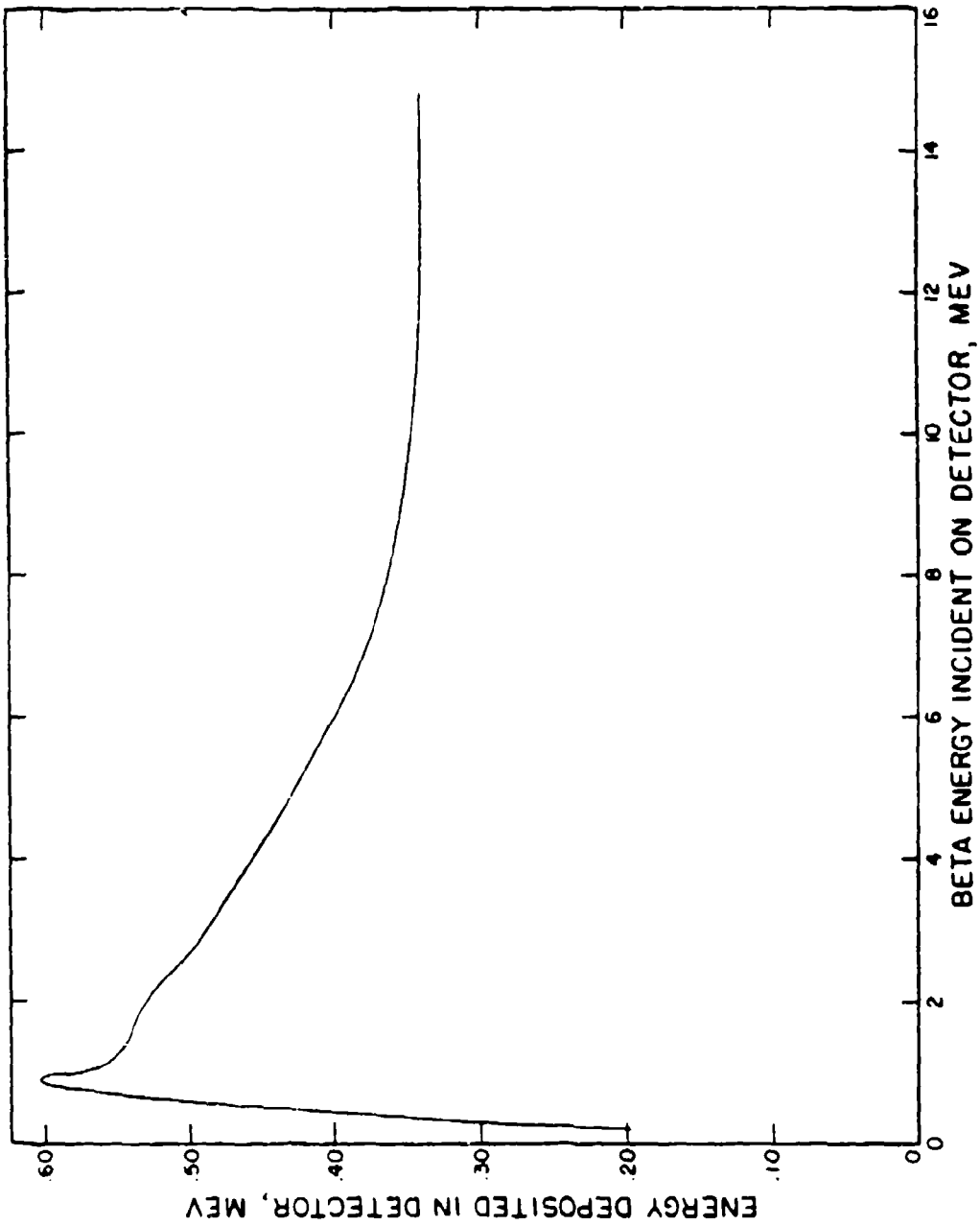

Figure 2.9 Beta detector energy calibration.

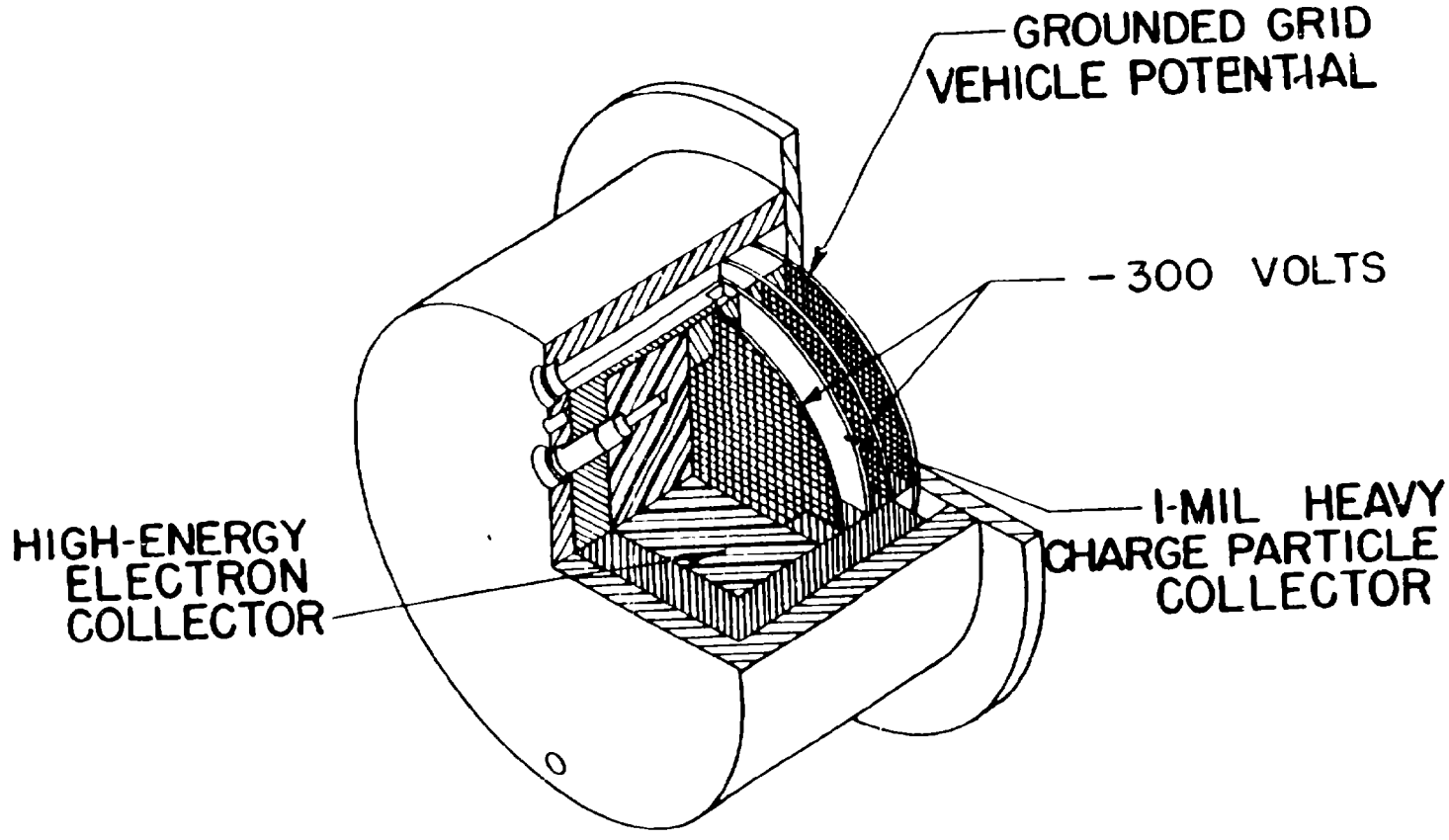

Figure 2.10 Faraday cup.

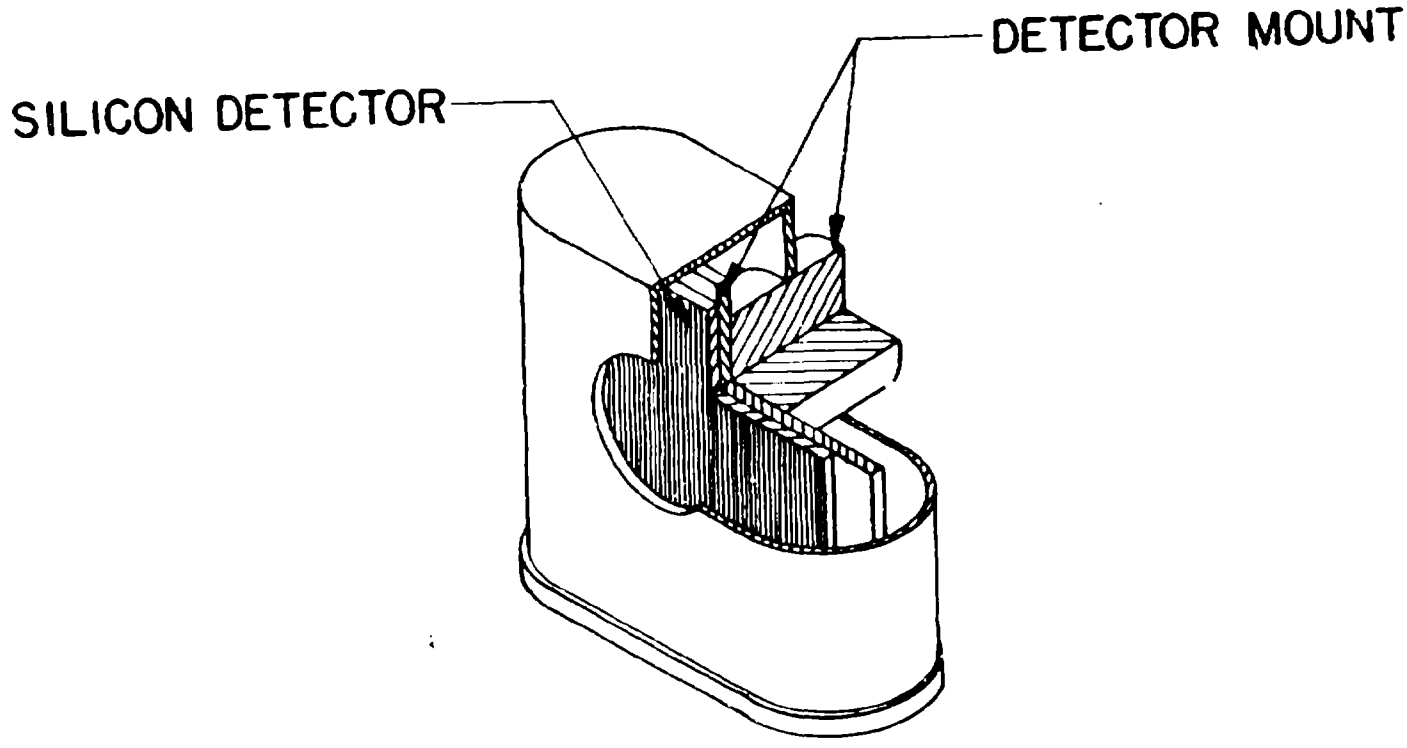

Figure 2.11 Gamma-neutron detector.

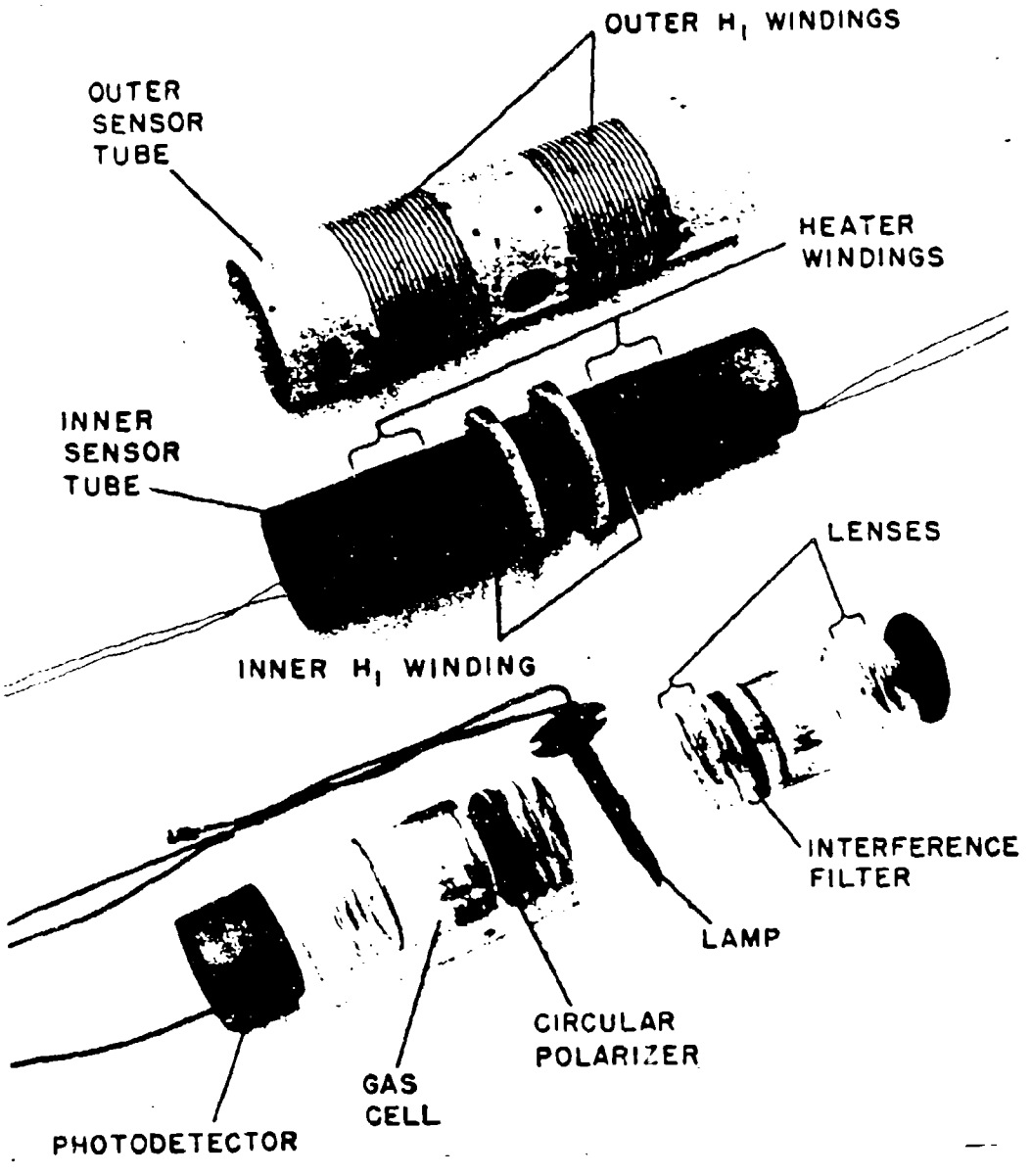

Figure 2.12 Rubidium vapor magnetometer. (AFWL photo)

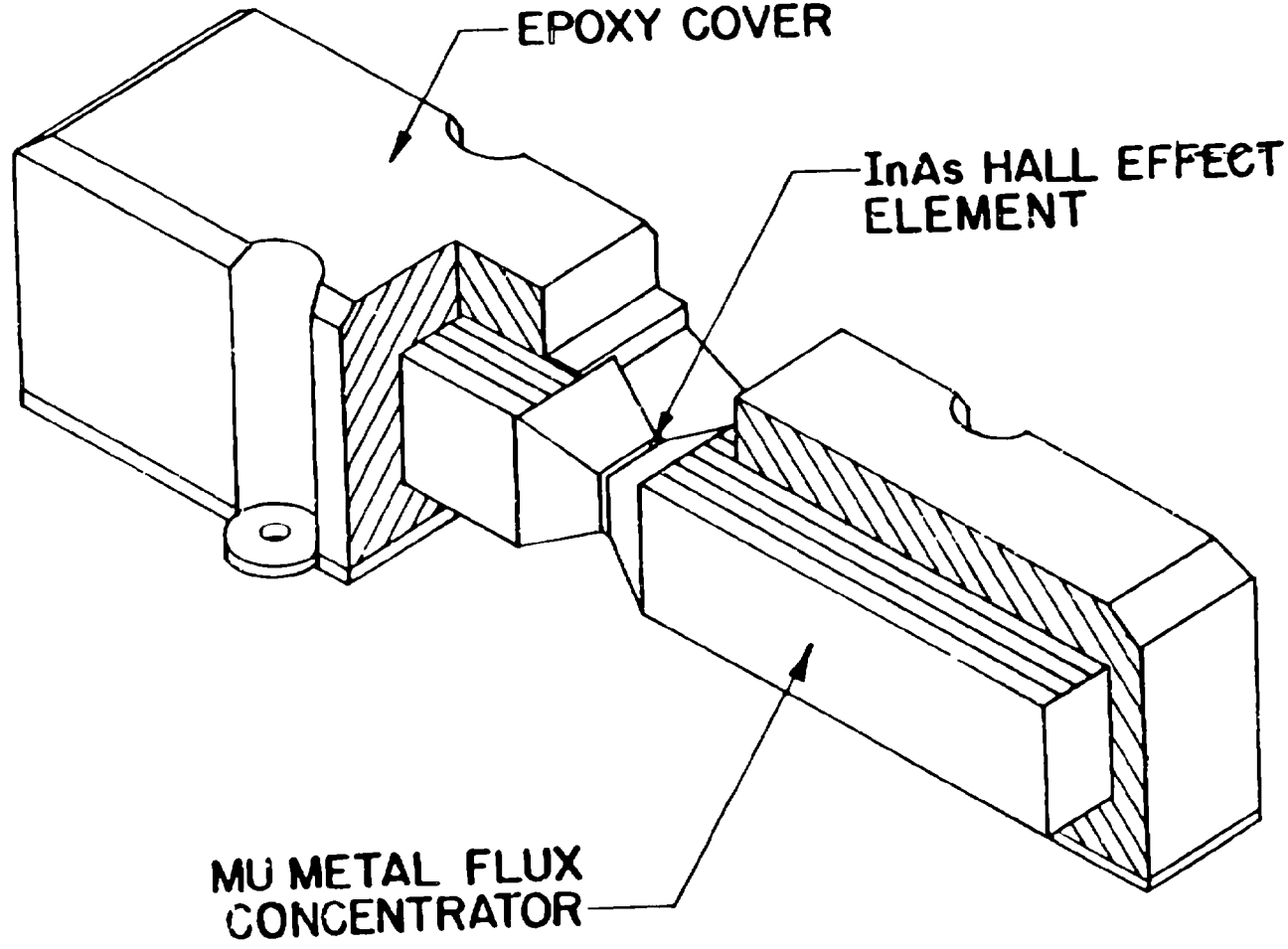

Figure 2.13 Hall effect magnetometer.

CHAPTER 3

RESULTS

3.1 STAR FISH

3.1.1 Star Fish Instrument Positions. Figure 2.1 shows the rocket trajectories in the magnetic meridian through Johnston Island at the time of the Star Fish event. The rockets are labeled as P-2, P-3, P-4, P-6, and P-7, and their positions at H-0 time are denoted by the initial part of a short, heavy line along the trajectory path. This short, heavy line represents the rocket position during the thirty seconds that the high-frequency data was stored in the tape recorder immediately following the burst. The launch azimuths were chosen so that the trajectories would follow the magnetic meridian through Johnston Island. Projections of these trajectories upon the earth's surface are shown in Figure 2.2. The five islands which had receiving sites for Project 6.7 rockets are also shown in Figure 2.2, and positions at H-0 time are denoted by an "X" along each trajectory. Because rocket pairs P-7, P-2 and P-4 and P-3 were launched with identical azimuth settings, their separation is not resolvable in Figure 2.2. The RF blackout data and real-time radiation fluxes are evaluated by using the altitude vs. time plot which is shown in Figure 2.3, and the exact distances at H-0 time which are given in Table 4.1. The rockets were programmed to be 100, 200, 400, and 800 km across the field lines through the burst at H-0 time. These distances, based on previously

mentioned calculations, were chosen so that debris ionization percentages could be measured. For example, the Rocket P-7 should be near the stopping radius point if the material were only 10% ionized and Rocket P-6 if it were only 1% ionized.

3.1.2 Position P-6 Measurements. Payload P-6 was located 117 km down and across the field lines from the burst point. Measurements obtained from the instruments at times from H-0 to H+30 seconds are shown in Fig. 3.1. Proceeding from the top to the bottom of Figure 3.1, the five plots represent the outputs of the following instruments:

(1) Faraday cup thick collector

(2) The 1-mil Faraday cup foil

(3) Solid-state beta detector

(4) Solid-state gamma-neutron detector

(5) Rubidium vapor magnetometer

The top graph in Figure 3.1 gives the results from one of the three Faraday cup foils located aboard Payload P-6. This foil was located behind a grounded grid and a grid biased at -300 volts to keep out the low-energy plasma electrons and allow measurements of only positively charged heavy particles. The instrument was capable of measuring ion fluxes from plus and minus 10^5 to 10^{14} charges per cm^2/sec/ster. The first downward deflection was caused by the transient radiation effect from the prompt gammas. The subsequent negative charges, measured from 10^{-3} to 10^{-1} second, are probably due to electrons with energies greater than 300 ev. At H+0.755 second, the Faraday cup foil goes from a negative current reading

to a large positive current reading. This is interpreted to be the arrival time of those positively charged heavy debris ions, which traveled with a velocity of

The second graph from the top in Figure 3.1 gives the results of one of the three thick Faraday cup electron detectors located aboard Payload P-6. The ordinate has the units of charge times 2.47 cm^2/sec/ster. The abscissas, common to all graphs in Figure 3.1, are times in seconds after H-0. The thick aluminum collector located behind the thin foil in the Faraday cup was designed to measure the high-energy fission product beta particles. The electrometer used to measure the current from this thick collector also experienced a severe transient radiation effect and did not recover until H+.002 second. At H+51 milliseconds, the Faraday cup detected a large negative current in the thick collector which is interpreted to be the arrival of the high-energy beta particles. At H+13 seconds, there was a sharp decrease in intensity of these beta particles, and the intensity is modulated in time at twice the spin rate of the vehicle.

The third graph from the top in Figure 3.1 represents the output of one of six lithium ion drifted solid-state beta detectors aboard Payload P-6. The amplifier in this instrument also experienced transient radiation effects until H+1 millisecond. At this time the electronics recovered and was able to measure the 14-Mev fusion neutrons which arrived after the prompt gammas. The solid-state detector then measured the lower energy fission neutrons and delayed gammas until at which time

a high flux of beta particles arrived at the P-6 position. From the center graph in Figure 3.1, it is evident that the beta particles were expanding outward in the form of a shell traveling with an average velocity of

At H+16.7 seconds the beta detector output was intensity modulated at twice the spin rate of the vehicle (Figure 3.11). This modulation is due to the beta particles being trapped in the magnetic field which is orthogonal to the vehicle spin axis.

The fourth graph from the top in Figure 3.1 gives the result of the gamma-neutron detector on board Payload P-6. The results are plotted as R/second deposited in silicon vs. time. Prompt gammas from the bomb caused the first peak to occur at about H+2 milliseconds. It was delayed in time because the telemetry frequency response was slower than a millisecond. At H+1.85 milliseconds, 14-Mev fusion neutrons arrived and caused a larger increase in R per second than the prompt gammas. The difference between the arrival times of the prompt gammas and the 14-Mev fusion neutrons made possible a comparison between the distance from the burst point as measured by radar and the distance as measured by neutron time-of-flight. Using the relativistic kinetic energy of the 14.5-Mev neutrons to be

$$KE = 939.526 \quad (1-V^2/C^2)^{-1/2}-1$$

where V is the velocity of the neutrons and C the velocity of light. The distance from the burst point to the payload is given by the following expression:

$$d = t_{\gamma-n^o} V_{n^o} (1-V_{n^o}/C)^{-1}$$

where $t_{\gamma\text{-}n^o}$ is the time between the arrival of the prompt gammas and the neutrons. The flux deposited in the gamma neutron detector following the 14-Mev neutrons was due to lower energy fusion neutrons and delayed gammas from the radioactive fission debris.

The bottom graph in Figure 3.1 gives the results of the Rb^{85} magnetometer. The magnetic field remained constant at the ambient value of 0.29 gauss until H+51 milliseconds at which time the transient radiation effect rendered the instrument inoperable. At H+2.5 seconds the instrument recovered and proceeded to measure the magnetic field until H+25 seconds. The field rapidly returned toward the ambient value at H+16 seconds and simultaneously the beta intensity was modulated at twice the 2.5-cycle/sec vehicle spin rate, indicating that the betas were trapped in the magnetic field. The angular distribution of beta particles, as measured by the six orthogonal beta detectors, was isotropic inside the expanding plasma bubble.

Figure 3.2 shows the outputs of the Faraday cup foil and the high-energy beta detector for the entire flight of the payload. The top graph in Figure 3.2, showing the Faraday cup foil output, indicates that the payload passed through a region of maximum ionization at 300 km. Immediately following the detonation, it measured the shell of expanding positive ions, and then for the remainder of the flight, measured more negative than positive charges. The beta detector saw a sharp increase in beta intensity immediately following the detonation and gradually fell off in intensity after the fission debris shell had passed beyond the payload.

3.1.3 Position P-3 Measurements. Payload P-3 was located 205 kilometers down and across the field lines from the burst point. Measurements obtained from the instruments at times from H-0 to H+30 seconds are shown in Figure 3.3. Proceeding from the top to the bottom of Figure 3.3, the five plots represent the outputs of the following instruments:

(1) Faraday cup thick collector

(2) The Faraday cup foil

(3) Solid-state beta detector

(4) Solid-state gamma-neutron detector

(5) Rubidium vapor magnetometer

The top graph in Figure 3.3 gives the results of one of the three Faraday cup foils located aboard P-3. This foil was located behind the grounded grid and a grid biased at -300 volts; thus, it kept out low-energy plasma electrons and measured only positively charged, heavy particles. The instrument was capable of measuring ion fluxes from plus and minus 10^5 to 10^{14} charges per cm^2/sec/ster. The negative current measured during the first 20 milliseconds after H-0 was probably caused by Compton electrons, and the first positively charged material was due to the ionized air. At H+6 seconds, the Faraday cup foil detected positive particles in one direction and negative charges in another direction. This was probably due to high-energy betas that penetrated the plasma sheaths surrounding the vehicle.

The second graph from the top in Figure 3.3 gives the results from one of the three thick Faraday cup electron detectors located

aboard Payload P-3. This thick aluminum collector was located behind the thin foil in the Faraday cup and was designed to detect and stop the high-energy fission beta particles below 7 Mev.

The third graph from the top in Figure 3.3 represents the output from one of the six lithium drifted solid-state detectors aboard Payload P-3. The first peak at about 8×10^{-4} second was due to the prompt gammas from the device, while the peak 3.18 milliseconds later was due to the 14-Mev fusion neutrons. The energy deposited by the delayed gamma rays and lower energy neutrons fell off to the detector threshold value at 1 second. At H+2.57 seconds the beta detector measured a flux of high-energy beta particles which were trapped in the magnetic field as shown in Figure 3.11. This flux lasted for 1.3 seconds. At H+5.27 seconds, a 4-second duration flux of trapped beta particles was detected, and later at H+13.5 seconds the rocket entered the plasma bubble. This penetration occurred when the rocket was at an altitude of 271 kilometers and the flux decreased sharply within 17 seconds as seen in Figure 3.4. This corresponded to an altitude of 301 kilometers.

The fourth graph from the top of Figure 3.3 gives the results from the gamma-neutron detector for Payload P-3. The results are plotted as R per second deposited in silicon vs. time. The first peak from prompt gammas, at about H+2 milliseconds, was delayed since the telemetry channel signal response was limited to 1 millisecond. At H+3.18 milliseconds, the 14-Mev neutrons arrived and were followed immediately by the lower energy fission neutrons

and delayed gammas. At about H+10 seconds another increase in gamma flux was measured during rocket penetration of the radioactive debris.

The bottom graph in Figure 3.3 gives the results of the Rb^{85} magnetometer. The magnetic field remained constant at its ambient value of about .31 gauss until H+1.0 second; then, a transient radiation effect turned off the magnetometer. At H+3 seconds, the instrument recovered and measured the magnetic field until H+25 seconds. The magnetometer output frequency, as measured by the telemetry receiver, could represent one of three magnetic field values. During the time of the dead zone in the magnetometer measurement, information was lost which would have allowed a unique determination of the magnetic field value represented by the measured frequency. Thus, the bottom graph in Figure 3.3 could represent an increase rather than a decrease in the magnetic field.

Figure 3.4 shows the output of the Faraday cup foil and the high-energy beta detector for the entire flight of the payload. The top graph in Figure 3.4, showing the Faraday cup foil output, indicates that the payload passed through a layer of ionized material which was probably caused by the debris stopped on top of the ionosphere; subsequently, a negative charge was detected due to high-energy electrons. This is similar to measurements taken aboard Payload P-6. The lower graph in Figure 3.4 shows that the payload passed through a region containing high-energy beta particles from H+13.5 seconds to H+30 seconds. These times correspond to rocket altitudes of 271 kilometers and 301 kilometers, which can be interpreted as being a layer of stopped radioactive debris.

3.1.4 Position P-7 Measurements. Payload P-7 was located 414 kilometers up and across the field line from the burst point. Measurements obtained from the instruments from H-0 to H+50 seconds are shown in Figure 3.5. Proceeding from the top to the bottom of Figure 3.5, the five plots represent the outputs of the following instruments:

(1) The Faraday cup heavy-particle detector

(2) Faraday cup high-energy electron collector

(3) Solid-state beta detector

(4) Solid-state gamma-neutron detector

(5) Rubidium vapor magnetometer

The top graph in Figure 3.5 gives the results from one of the three Faraday cup foils located aboard P-7. The foil was designed to measure ion fluxes from plus and minus 10^5 to 10^{14} charges per cm^2/sec/ster. The foil measured a large flux of positive ions which started at about H+1.20 seconds and continued for 400 seconds. The arrival time implied an average velocity of 345 kilometers per second for the positively charged debris. The dotted line starting at H+1.7 seconds in the top graph of Figure 3.5 is the envelope of the high-energy betas modulated at the spin rate of the payload.

The second graph from the top in Figure 3.5 gives the results of one of the three high-energy electron Faraday cup detectors located aboard Payload P-7. This thick aluminum detector, located behind the thin foil in the Faraday cup, measured a large flux of electrons starting about H+0.480 second.

The third graph from the top in Figure 3.5 represents the output from one of the six lithium drifted solid-state detectors aboard Payload P-3. The first peak at about 5×10^{-4} second was due to the prompt gammas from the device, and the peak intensity 6.57 milliseconds later was due to the 14-Mev fusion neutrons. At H+480 milliseconds a sharp increase in beta flux intensity was measured which subsequently fell rapidly at 4.3 seconds. The betas measured after 4.3 seconds were trapped by the magnetic field as indicated in Figure 3.11. This occurred simultaneously with the recovery of the magnetic field. The arrival time of high-energy beta particles at H+480 milliseconds implies an average expansion velocity of 862 kilometers per second for the shell of high-energy betas.

The fourth graph from the top of Figure 3.5 gives the results from the gamma neutron detector for Payload P-7. The first peak which occurred at about H+2 milliseconds was due to the prompt gammas from the bomb. A second peak occurred 6.57 milliseconds later and was due to the 14-Mev fusion neutrons. A shell of radioactive debris ions caused a third peak in gamma intensity at H+0.2 second.

The bottom graph in Figure 3.5 shows the output of the Rb^{85} magnetometer on Payload P-7. A timer malfunction caused data to be lost from H-0 to H+2.9 seconds. The ambient field of 0.27 gauss at H-0 time is denoted by a dot in the upper left hand corner of this plot. The bottom graph shows that the magnetic field returned toward ambient value at 4.3 seconds. Simultaneously with this return

toward the ambient magnetic field, the high-energy beta particles were trapped as shown in Figure 3.6. The radioactive shell of delayed gamma emitters had passed the payload as shown in the gamma detector measurement.

3.1.5 Position P-2 Measurements. Payload P-2 was located 807 kilometers up and across the magnetic field lines from the burst point. Measurements obtained as a function of time after detonation are shown in Figure 3.7. Proceeding from the top to the bottom in Figure 3.7, the three plots represent the outputs of the following instruments:

(1) Faraday cup foil

(2) Solid-state beta detector

(3) Rubidium vapor magnetometer

The top graph of Figure 3.7, which shows the Faraday cup foil heavy-particle detector results, was noisy from H-0 to H+0.6 second. The information at 0.6 second shows the positive ion density to be substantially increased over ambient conditions. The high-energy beta detector results, shown in the center graph of Figure 3.7, indicate a large flux of beta particles arriving at H+19.9 seconds. All beta particles detected by Payload P-2 were trapped in the geomagnetic field. The bottom graph in Figure 3.7 shows the magnetic field as measured by the Rb^{85} magnetometer. The magnetometer experienced no transient radiation effects, since the payload was far removed from the detonation point. The magnetic field started to increase in value at H+4 seconds. This increase in magnetic field at the

Payload P-2 position indicates that a diamagnetic bubble was formed and subsequently decayed without having the plasma boundary pass the P-2 payload position. Figure 3.8 shows the real-time beta and ion flux at the P-2 payload position for the total duration of the flight. The Faraday cup ion detector measured the highly ionized region at 320 kilometers. After passing through this region a net negative current was measured until the detonation of the weapon, at which time a net positive charge was measured until the rocket re-entered the atmosphere. The high-energy beta detector, shown in the lower graph of Figure 3.8, measured a high flux of beta particles starting at H+19 seconds and rapidly fell off in intensity at H+60 seconds. The flux of beta particles then slowly decayed below the threshold value of the detector at H+200 seconds. These beta particles were 100% trapped in the magnetic field, since the beta intensity was modulated at twice the spin rate of the vehicle.

3.1.6 Position P-4 Measurements. Payload P-4 was located 1025 kilometers along the field line from the burst point. Measurements obtained from the instruments on this payload for thirty seconds following H-0 are shown in Figure 3.9. Proceeding from the top to the bottom of Figure 3.9, the five plots represent the outputs of the following instruments:

(1) Faraday cup heavy-particle detector

(2) Faraday cup high-energy electron detector

(3) Solid-state beta detector

(4) Solid-state gamma-neutron detector

(5) Rubidium vapor magnetometer

The top graph in Figure 3.9 gives the results from one of the three Faraday cup foils located in Payload P-4. This foil measured a large flux of electrons with energies greater than 300 ev at H+0.2 second. At H+1.55 seconds the foil detected a large flux of positive ions. The dotted line represents the envelope of the nagatively charged particle measurements which were intensity modulated at the spin rate of the vehicle. The arrival time of positive ions at 1.55 seconds indicates an average velocity of 662 kilometers per second for this expanding material.

The second graph from the top in Figure 3.9 gives the results from one of the three high-energy electron Faraday cup detectors. This detector measured a large flux of high-energy electrons starting at 455 milliseconds.

The center graph in Figure 3.9 gives the results from one of the six solid state beta detectors aboard Payload P-4. The first two peaks represent the arrival of the prompt gammas and the 14-Mev fusion neutrons, respectively. At H+.455 second, the beta detector measured a sharp increase in high energy beta flux. This time of arrival indicates an average velocity of 2203 kilometers per second for the expanding shell of high energy betas. These beta particles were modulated at the spin rate of the vehicle from H+0.455 second to H+2.29 seconds at which time the intensity modulation changed from 2.5 cycles per second to 5 cycles per second as shown in Figure 3.11.

The 5-cycle/sec intensity modulation of the beta particles occurred simultaneously with the recovery of the magnetic field and has been interpreted to indicate the start of electron trapping.

The fourth graph from the top of Figure 3.9 gives the results from the gamma neutron detector for Payload P-4. The time between the first and second peaks is 16.26 milliseconds and represents the flight time of the 14-Mev fusion neutrons. The resultant increase in gamma flux a H+455 milliseconds has been interpreted as the arrival of the radioactive shell of debris ions.

The bottom graph in Figure 3.9 shows the output of the Rb^{85} magnetometer on Payload P-4. The magnetic field remained at the ambient value of 0.22 gauss until H+0.68 second. At this time the gamma flux was high enough to cause transient radiation effects in the rubidium magnetometer electronics. The magnetometer recovered from these effects at H+1 second and measured a decrease in the magnetic field followed by an increase toward ambient conditions at H+2.4 seconds. Simultaneously with this magnetic field recovery, the angular distribution of high-energy beta particles changed from isotropic to anisotropic and peaked at 90° to the magnetic field lines.

Figure 3.10 shows the results from the Faraday cup foil and the high-energy beta detector during the entire flight of Payload P-4. The faraday cup foil first measured the ions in the region centered about 320 kilometers and subsequently measured a large increase in positive ions which followed the detonation of the

weapon. The high-energy beta detector first measured an expanding shell of beta particles which was traveling at 2,253 kilometers per second and then a flux of beta particles which slowly decreased in intensity as the rocket proceeded along the field line. The slow decrease in trapped beta intensity was probably due to the collapse of the magnetic field which allowed the high-energy betas to escape through the neck of the magnetic bottle along the field line. The time history of the intensity of the beta flux was strongly dependent upon the trajectory of the rocket, because the rocket did not follow the field line to the southern conjugate point.

3.1.7 Hall Effect Magnetometer Measurements. The Hall effect magnetometer measured the vector component of the magnetic field along the spin axis of each rocket. This magnetometer had a range from plus and minus 0.03 to 4 gauss with an overload capability of ± 6 gauss. The early time results from the Hall magnetometer measurements are shown in Figure 3.12. The large changes near H-0 are caused by the transient radiation effects on the amplifier used in this device. A cursory look at the magnetometer signals indicates that significant field changes were measured only by Payload P-6. This field occurred simultaneously with the arrival of the high-energy beta particles at H+51 seconds and lasted for 12 milliseconds. This may be a magnetic shock, but it is also possible that the pulse was caused by the transient radiation effect in the amplifier. Although this magnetometer has been calibrated in a radiation environment, the data is still in the reduction process.

3.1.8 Johnston Island Magnetometer. A spare payload was

operated on Johnston Island during the Star Fish event. Fifteen minutes of rubidium vapor magnetometer information was recorded starting 7.5 minutes before H-0 and ending 7.5 minutes after H-0. Figure 3.13 shows the magnetic field measured on Johnston Island as a function of time after the Star Fish burst. Though the amplitude was not accurate, the first large increase at time H-0 was due to the EMP. The next increase from the ambient field of 0.3425 gauss to 0.3440 gauss occurred at H+3.6 seconds. This was followed by a second increase to 0.3454 gauss which peaked at H+25 seconds. A slow decrease in field to 0.3355 gauss at H + 65 seconds was subsequently followed by a return to the ambient field at H + 400 seconds. The last large decrease of 700 gamma occurred at H + 65 seconds and can be correlated with the Edgerton, Germeshausen, and Grier, Inc., (EG&G) measurements on Check Mate and King Fish (Reference 12). The magnetometer signals measured on Johnston Island had approximately the same shape, but the amplitudes and times were strong functions of bomb altitude and yield. In all three cases, the field had two increases followed by a slow decrease and subsequent recovery to ambient conditions. It may be fortuitous, but the last slow decrease in field for the three highest altitude shots was directly proportional to the yield of the devices.

3.1.9 RF Attenuation Measurements. Receiving sites for the Star Fish event were located on Johnston, Oahu, Hawaii, Tern, and Canton

Islands. These sites are shown in Figure 2.2 along with the rocket trajectories projected onto the earth's surface. Frequencies transmitted by the payloads were as follows:

P-2	247.3	Megacycles
P-3	237.0	"
P-4	229.0	"
P-6	221.5	"
P-7	216.5	"

Figure 3.14 shows the signal strength records received at Johnston Island from H-1 to H+100 seconds. The receiving system on Johnston Island had a 30-db dynamic range and used an antenna with a 13-dbm gain. This system was designed for payload check-out and was used only as a backup for payload reception. The signal strength measured at Johnston Island decreased to receiver noise levels immediately at H-0 and recovered at about H+7 seconds.

The signal strength as measured from outlying sites on Star Fish are shown in Figure 3.15. Since these receiving sites used 18- to 28-dbm gain antennas, blackout was not as severe as experienced at Johnston Island. The RF signals were all blacked out at H-0 but recovered in about a half a second to levels high enough to obtain good data. The blackout duration and recovery time was a strong function of the relative position of the signal transmission path and the ionized regions produced by the bomb.

3.2 CHECK MATE

3.2.1 Check Mate Instrument Positions. Two rockets were used on Check Mate to position Payloads P-1 and P-5 at 101 kilometers

along the field line from the burst and at 112 kilometers above the burst at H-0 time, respectively. These payloads were duplicates of those used for the Star Fish event, and the trajectories are shown in Figure 3.16. This represents a slice in the magnetic meridian through Johnston Island, and the extra heavy solid line indicates the position of the payloads at time H-0. A projection of the trajectories onto the earth's surface is shown in Figure 3.17, and the positions of the payloads at H-0 are denoted by an "X" along the flight path. Figure 3.17 also depicts the islands that were used as receiving sites for the two payloads. The time vs. altitude curve is shown in Figure 3.18 with H-0 time occurring at 30,600 seconds.

3.2.2 Position P-1 Measurements. Payload P-1 was located 101 kilometers along the field line and up from the burst point. Flux measurements obtained as a function of time from the instruments in this payload are shown in Figure 3.19. Proceeding from the top to the bottom of Figure 3.19, the five plots represent the outputs of the following instruments:

(1) Faraday cup thick collector

(2) The 1-mil Faraday cup foil

(3) Solid-state beta detector

(4) Solid-state gamma-neutron detector

(5) Rubidium vapor magnetometer

The top graph in Figure 3.19 shows the results from one of the three Faraday cup foils located in Payload P-1. This foil measured

a large flux of electrons with energies greater than 300 ev immediately following H-0, and at H+20 milliseconds the foil started to detect a large flux of positive ions. This positively charged flux was measured until H+0.1 second at which time a large flux of negative particles was measured. This negative flux could be due to Compton electrons which were detected as the Faraday cup turned and faced the nuclear fireball. The angular coordinates with respect to the fireball origin were not determined in the initial phase of data reduction. The next large flux of positive ions occurred at H+.25 second which indicated an average ion velocity of 400 kilometers per second over the flight path of 101 kilometers.

The second graph from the top on Figure 3.19 shows the results from one of the three high-energy electron Faraday cup detectors. This thick collector detected a negatively charged flux at H+0.01 second and continued to measure this flux until a decrease occurred at H+20 seconds. The center graph Figure 3.19 shows the results from one of the six solid-state beta detectors located in Payload P-1.

At H+6 seconds this distribution changed to an anisotropic angular distribution with the flux values peaked at 90° with respect to the magnetic field lines.

The fourth graph from the top in Figure 3.19 shows the results from the gamma-neutron detector located behind the nylon bremsstrahlung shield. The two peaks represent the arrival of the prompt gammas and the 14-Mev fusion neutrons, respectively.

The bottom graph in Figure 3.19 shows results from the Rb^{85} magnetometer. The magnetic field started to decrease at the same time that the high-energy betas arrived at the payload position, and continued to decrease until a minimum was reached at H+0.455 second. The magnetic field then recovered to its ambient value at H+1.25 seconds. The subsequent decrease, as shown in Figure 2.19, is due to the rocket traveling out to lower values of the earth's magnetic field.

The results from the Faraday cup ion detector and the solid state high energy beta detector are shown in Figure 3.20 as a function of time for the entire flight of the payload. The top graph of Figure 3.20 shows that the Faraday cup foil measured a large flux of positive ions immediately following the detonation for about 500 seconds. The beta detector results, shown in the bottom graph of Figure 3.20, indicate that the large flux of beta particles which started at H+63 milliseconds dropped immediately to near ambient values at H+2 seconds.

3.2.3 Position P-5 Measurements. Payload P-5 was located 112 kilometers directly above the burst point. Measurements obtained from the instruments in this payload for a period of thirty seconds following H-0 are shown in Figure 3.21. Proceeding from the top to the bottom of Figure 3.21, the five plots represent the out-

puts of the following instruments:

(1) Faraday cup thick collector

(2) The 1-mil Faraday cup foil

(3) Solid-state beta detector

(4) Solid-state gamma-neutron detector

(5) Rubidium vapor magnetometer

The top graph in Figure 3.21 shows the output of the Faraday cup foil heavy ion detector. There was an increase in positive ion flux at H+0.14 second, and this ion intensity was modulated at the spin rate of the vehicle. The second graph from the top of Figure 3.21 gives the results from one of the three high-energy Faraday cup detectors. The thick collector located behind the Faraday cup foil measured three peaks of the positive ion current at H+2, 8, and 20 milliseconds. The center graph in Figure 3.21 gives the output of the high-energy solid-state beta detector. This detector measured the arrival of the prompt gammas which was followed 1.84 milliseconds later by the 14-Mev fusion neutrons. No beta flux was measured by this detector.

The results from the gamma-neutron detector are shown on the fourth graph from the top in Figure 3.21. This detector measured a time separation of 1.84 milliseconds between the arrival of the prompt gamma and the fusion neutrons. No gamma ray flux intensity exceeded the instrument threshold after passage of the 14-Mev fusion neutrons.

The bottom graph in Figure 3.21 shows the results from the Rb^{85} magnetometer measurements. The vehicle experienced an R^{-3} drop-off

in magnetic field intensity as it proceeded out from the earth's surface. Since R^{-3} reduction in field has not been subtracted, the lower graph in Figure 3.21 may contain some very low perturbed field information after H-0.

Figure 3.22 shows the output of the Faraday cup foil and beta detector as a function of time during the entire flight of the payload. The high-energy beta particle flux did not exceed the threshold of the beta detector at any time during the flight of Payload P-5. The ion intensity, shown in the top graph of Figure 3.22, increased in positive value following H-0. It subsequently decreased due to an increase in negatively charged ion flux. The measurements shown in Figure 3.21 indicate that the radioactive bomb debris did not reach this payload during the flight time.

3.2.4 RF Attenuation Measurements. Payloads P-1 and P-5 transmitted 10 watts of RF energy at 229.9 and 231.9 megacycles, respectively. Receiving sites were located at Canton, Johnston, Tern, and Oahu Islands during the Check Mate event. Figures 3.23 and 3.24 show the signal strength records as measured on Johnston and Tern Islands from H-1 to H+100 seconds. The signal strength from Payload P-1, as measured on Johnston Island, decreased sharply at H+1 second when the ionized plasma expanded into the line-of-sight path from the antenna to the payload.

Pages 63 through 86 deleted.

CHAPTER 4

DISCUSSION

4.1 STAR FISH DEBRIS HISTORY

Table 4.1 is a synopsis of the time-dependent quantities measured by Project 6.7 instrumentation. These measurements indicate that the debris expanded unimpeded along the field lines for thousands of kilometers, but that this debris was drastically slowed as it traversed across the field lines. The debris was probably stopped at an altitude between 500 to 800 kilometers above the burst point and 270 kilometers below the burst point. Figure 4.1 shows the rocket trajectory and also an estimate of the plasma bubble surface at H+0.051 second and H+0.480 second. This bubble probably expanded for approximately 1 second and subsequently collapsed, squirting the ionized material and high-energy beta particles down along the field lines toward the northern and southern magnetic conjugate regions. Previous estimates made in Section 1.3 indicate that the percentage of debris ionized was between 10 and 100%. The radioactive debris particles injected betas at high enough L values (Reference 13) to take the high-energy electrons over the southern magnetic anomaly and produced a long-lasting belt of electrons around the earth. Figure 4.2 shows the center of this artificial belt as measured by Van Allen (Reference 14) from satellite INJUN I detectors. Approximately 5 to 10% of the total high-energy beta particles were injected at high enough L values to pass this magnetic

field anomaly. Satellite measurements placed the center of the long-lived artificial belt at an L value of 1.2. Most of the high-energy betas injected along the field line through the burst point were deposited in the atmosphere at the northern and southern magnetic conjugate regions.

It is recommended that more rocket payloads be used in future experiments involving asymetric weapon expansions.

4.2 CHECK MATE DEBRIS HISTORY

Table 4.2 is a synopsis of the Check Mate debris expansion.

4.3 DATA REDUCTION

The information on magnetic tapes as received by the telemetry sites was reduced by a digitized process which used an Astro Data A/D converter and a CDC 1604 computer. Most of this data is included in this report. Detailed reactor calibration data which is presently being reduced will allow a more accurate determination of the flux, energy, and angular distributions of the debris parameters. This voluminous calibration data and more detailed flux information will appear in a future report.

TABLE 4.1 STAR FISH DEBRIS EXPANSION

Rocket	Distance from Burst	Prompt Gamma Arrival Time	14-Mev Fusion Neutron Arrival Time	Fission Beta Arrival Time	Fission Beta Shell Velocity	Ion Arrival Time	Ion Velocity	Magnetic Field Recovery Time	Fission Beta Trapping Time
	km	msec	msec	sec	km/sec	sec	km/sec	sec	sec
P-6	117	0.39	1.85					16	16.7
P-3	205	0.67	3.18					—	2.57
P-7	414	1.38	6.57					4.3	4.3
P-2	807	Not Meas.	Not Meas.					4.0	19
P-4	1025	3.42	16.26					2.4	2.3

TABLE 4.2 CHECK MATE DEBRIS EXPANSION

Rocket	P-1	P-5
Distance from Burst at H-0	101 km	112 km
Prompt Gamma Arrival Time	0.34 msec	0.35 msec
14-Mev Fusion Neutron Arrival Time	1.60 msec	1.84 msec
Fission Beta Arrival Time		Did Not Arrive
Fission Beta Shell Velocity		
Ion Arrival Time		
Ion Velocity		Data Not Reduced
Magnetic Field Recovery Time	0.8 sec	
Fission Beta Trapping Time	6.0 sec	

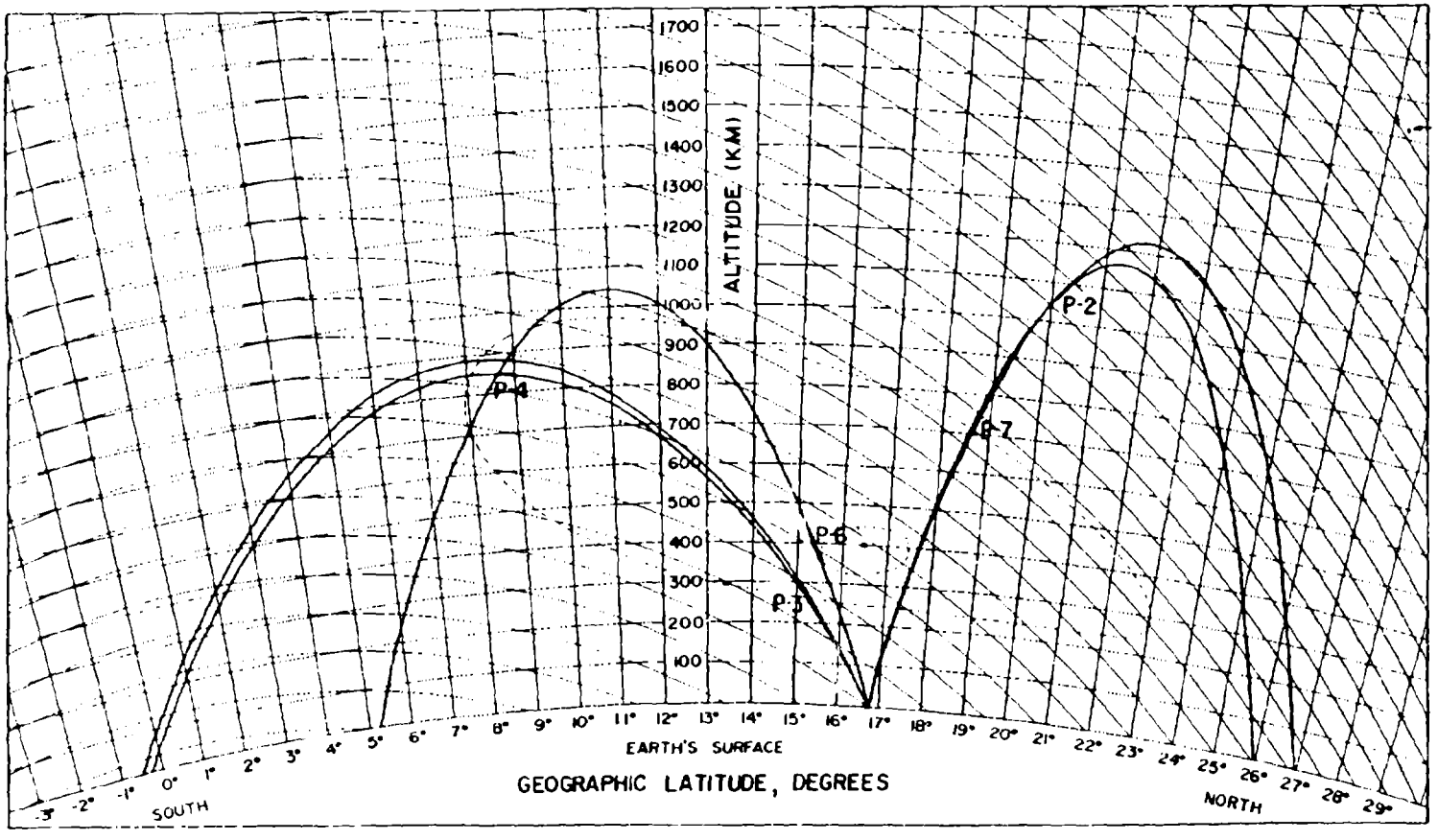

Figure 4.1 Star Fish debris expansion.

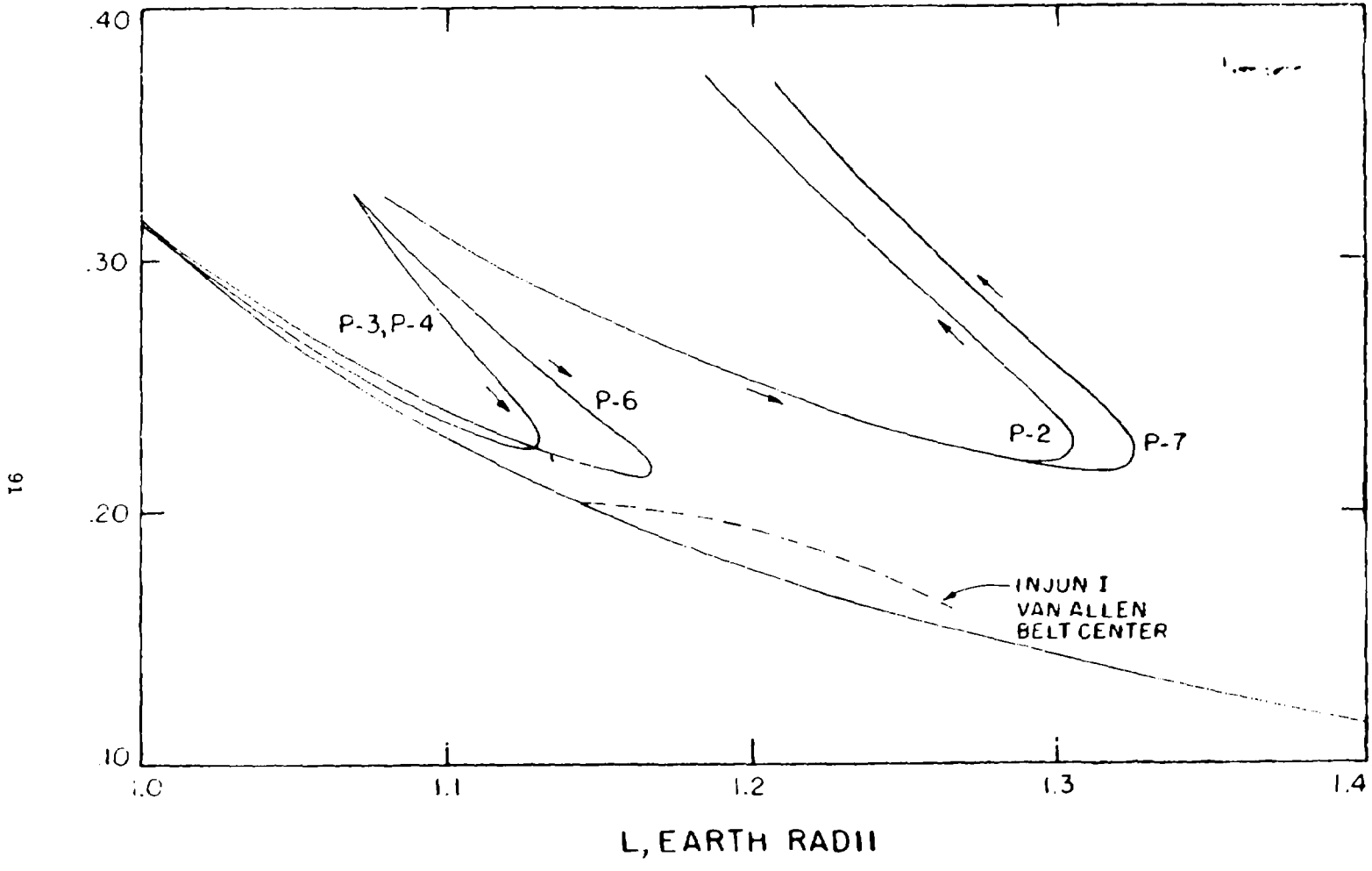

Figure 4.2 B, L plot with Star Fish belt and 6.7 trajectories.

REFERENCES

1. A.L. Latter, and R.E. LeLevier; "The Pancake Shot (U)"; RM-2361, April 1959; The RAND Corporation, Santa Monica, California; Secret Restricted Data.

2. H.L. Brode; "Theoretical Description of the Blast and Fireball for a Sea Level Megaton Explosion (U)"; RM-2248, September 1959; The RAND Corporation, Santa Monica, California; Secret Restricted Data.

3. C.L. Longmire; "Notes on Debris-Air-Magnetic Interaction"; RM-3386-PR, January 1963; The RAND Corporation, Santa Monica, California; Unclassified.

4. T.G. Cowling; "Magnetohydrodynamics"; Interscience Publishers, 1956; New York, New York.

5. D.I. Prickett; "Selected Fish Bowl Operational Measurements (U)"; FC/01640270, January 1964; Headquarters Field Command, Defense Atomic Support Agency, Sandia Base, New Mexico; Secret Restricted Data.

6. R.D. Cowan, et al; "Calculations on the Early Phases of the Star Fish, Blue Gill, and Urraca Explosions (U)"; LAMS-2749, March 1962; Los Alamos Scientific Laboratory, Los Alamos, New Mexico; Secret Restricted Data.

7. R.W. Hendrick, R.H. Christian, and P.G. Fisher; "Operation Fish Bowl Theoretical Estimates of Expected Phenomena (U)"; RM 62TMP-36, May 1962; General Electric Company, Santa Barbara, California; Secret Restricted Data.

8. W.A. Lokke; "The Radiated Flux and Debris Angular Distribution of Star Fish Prime (U("; UCID-4551, January 1963; Lawrence Radiation Laboratory, Livermore, California; Secret Restricted Data.

9. M.P. Shuler, et al; DASA Review Symposium Fish Bowl 1, 22 (1963), DASA 1449; Defense Atomic Support Agency, Washington, D.C.; Secret Restricted Data.

10. D.C. Jensen, and J.C. Cain, Unpublished, presented at April 1962 American Geophysical Union Meeting, Washington, D.C.

11. H.I. West; "The Beta Ray Spectrum of the Fission Products of U^{235} at 1 to 300 Seconds After Fission"; UCRL-6123, August 1960; Lawrence Radiation Laboratory, Livermore, California.

12. R. O'Rourke; "ELF, VLF, and Magnetic Measurements (U)"; DASA 1383, June 1963; Defense Atomic Support Agency, Washington, D.C.; Secret Restricted Data.

13. C.E. McIlwain; "Coordinates for Mapping the Distribution of Magnetically Trapped Particles"; Journal of Geophysical Research, 66, 3681-3691, 1961.

14. J.A. Van Allen, et al; "Satellite Observations of the Artificial Radiation Belt of July 1962"; Journal of Geophysical Research, 68, 619-627, 1963.

Pages 95 and 96 deleted.